Particle and Fibre Toxicology

RESEARCH

Open Access

Genome-wide DNA methylation sequencing reveals the involvement of ferroptosis in hepatotoxicity induced by dietary exposure to food-grade titanium dioxide

Jiaxin Shang[1†], Jun Yan[1†], He Lou[1], Rongshang Shou[1], Yingqi Zhan[1], Xiaoyan Lu[1,2,3,5*] and Xiaohui Fan[1,2,3,4*]

Abstract

Background Following the announcement by the European Food Safety Authority that the food additive titanium dioxide (E 171) is unsafe for human consumption, and the subsequent ban by the European Commission, concerns have intensified over the potential risks E 171 poses to human vital organs. The liver is the main organ for food-grade nanoparticle metabolism. It is increasingly being found that epigenetic changes may play an important role in nanomaterial-induced hepatotoxicity. However, the profound effects of E 171 on the liver, especially at the epigenetic level, remain largely unknown.

Methods Mice were exposed orally to human-relevant doses of two types of E 171 mixed in diet for 28 and/or 84 days. Conventional toxicology and global DNA methylation analyses were performed to assess E 171-induced hepatotoxicity and epigenetic changes. Whole genome bisulfite sequencing and further ferroptosis protein detection were used to reveal E 171-induced changes in liver methylation profiles and toxic mechanisms.

Results Exposed to E 171 for 28 and/or 84 days resulted in reduced global DNA methylation and hydroxymethylation in the liver of mice. E 171 exposure for 84 days elicited inflammation and damage in the mouse liver, whereas 28-day exposure did not. Whole-genome DNA methylation sequencing disclosed substantial methylation alterations at the CG and non-CG sites of the liver DNA in mice exposed to E 171 for 84 days. Mechanistic analysis of the DNA methylation alterations indicated that ferroptosis contributed to the liver toxicity induced by E 171. E 171-induced DNA methylation changes triggered NCOA4-mediated ferritinophagy, attenuated the protein levels of GPX4, FTH1, and FTL in the liver, and thereby caused ferroptosis.

Conclusions Long-term oral exposure to E 171 triggers hepatotoxicity and induces methylation changes in both CG and non-CG sites of liver DNA. These epigenetic alterations activate ferroptosis in the liver through NCOA4-mediated ferritinophagy, highlighting the role of DNA methylation and ferroptosis in the potential toxicity caused by E 171 in vivo.

Keywords E 171, Liver toxicity, Epigenetics, DNA methylation, Ferroptosis, Ferritinophagy

†Jiaxin Shang and Jun Yan have contributed equally to this work.

*Correspondence:
Xiaoyan Lu
luxy@zju.edu.cn
Xiaohui Fan
fanxh@zju.edu.cn
Full list of author information is available at the end of the article

Introduction

Titanium dioxide (TiO_2), a ubiquitous pigment, is annually produced in over 9 million tons for various sectors, such as coatings, paper, food, and medicine [1]. Food- and pharmaceutical-grade TiO_2 (E 171), used as a colorant and film coating agent, is present in over 3500 food products, including chewing gums, pudding, and chocolate [2–4]. In the United States, exposure to TiO_2 was estimated to be on the order of 1 mg/kg per day of Ti for adults, whereas estimates for children were two to four times this dose [5]. The European Commission banned E 171 as a food additive in the European Union (EU) following the risk assessment of the European Food Safety Authority (EFSA) which used a nano-specific methodology, i.e., taking into account the particulate nature of the material and the extensive presence of biopersistent nanoparticles, concluded that a concern for genotoxicity could not be excluded along with a potential for accumulation, immunotoxicity, inflammation, induction of aberrant crypt foci and neurotoxicity [6–8]. However, the United States government and Department of Agriculture disagreed with this decision [9], and E 171 was deemed a safe food additive by several agencies, including the United Kingdom's Food Standard Agency, Health Canada, and World Health Organization [10–12]. These assessments attributed the highest weight to toxicological studies in which food-grade TiO_2 was administered via the diet at very high concentrations through simple admixing of the dry material, whereas EFSA rated best the toxicological studies where E 171 was administered via oral gavage or drinking water after proper dispersion, since extensive agglomeration may prevent particle uptake resulting in no exposure [13].

E 171 is still widely used outside the EU. It is noteworthy that E 171 has been confirmed to enter the blood circulation of human volunteers through oral exposure [14]. The entry of E 171 into the bloodstream may pose a potential risk in vivo [15–18], necessitating further toxicity assessments, particularly on vital organs, using exposure methods that mimic human exposure scenarios.

Due to its unique organ structure and blood flow characteristics, the liver is the main target organ for nanoparticles entering the circulation [19]. Accumulated nanoparticles in the liver may elicit liver toxicity [20, 21]. DNA methylation is an epigenetic modification that can be altered in response to environmental changes, including exposure to nanomaterials [22–25]. It is increasingly being found that exposure to nanomaterials may trigger DNA methylation changes in the liver. For instance, graphene quantum dots induced global DNA methylation changes in zebrafish liver [26], oxidized graphene altered DNA methylation patterns in mouse liver [27], and our previous studies demonstrated that food-grade nanosilica elicited extensive DNA methylation changes at CG and non-CG sites in the liver of male, pregnant, and fetal mice [28, 29]. This indicates that the epigenetic effects of nanomaterials on the liver should be taken seriously. Recent studies disclosed that E 171 may accumulate in the liver, where TiO_2 particles were also detected in the deceased, implying that the liver is one of the main organs of E 171 deposition in humans [30–32]. These studies suggested that exposure to E 171 may have adverse effects on the liver and cause epigenetic changes. However, the epigenetic changes and liver toxicity mechanisms caused by dietary exposure to E 171 are not yet clear.

Ferroptosis is a form of autophagic cell death characterized by the accumulation of iron in cells and subsequent lipid peroxidation [33–36]. It plays an important role in liver inflammation, injury, and metabolic diseases [37–40]. Ferritin is the primary iron storage protein [41], which is degraded through the autophagic process (ferritinophagy) mediated by nuclear receptor coactivator 4 (NCOA4) to release free iron [33]. The increase of free iron in cells can promote further ferroptosis by increasing the accumulation of lipid peroxidation [42]. Glutathione peroxidase 4 (GPX4) is the key regulator of ferroptosis that can clear peroxidized phospholipids, while GPX4 inhibition results in lipid peroxidation accumulation and ferroptosis [35]. Epigenetic modifications play a critical role in the regulation of ferroptosis and autophagy [42–44]. High methylation of nuclear factor E2-related factor 2 (*Nrf2*) promoter can inhibit *Nrf2* expression, which in turn affects GPX4 levels [45]. The epigenetic regulation of GPX4 levels is a direct way to regulate ferroptosis [46]. Moreover, there is a close relationship between ferritinophagy and DNA methylation, as inhibiting ferritinophagy suppresses DNA demethylation [47], and the aberrant DNA methylation has been demonstrated to affect the expression of NCOA4, which in turn regulates ferritinophagy [48]. These indicated that epigenetic modifications, especially DNA methylation, play an important role in autophagy and ferroptosis processes. It is worth noting that nanomaterials may induce ferroptosis and subsequent toxic reactions in multiple organs, including the liver [49–52]. However, the role of DNA methylation in nanomaterial-induced ferroptosis is poorly understood. The effect of E 171 on ferroptosis and epigenetic mechanisms in the liver remains unclear.

In this study, we simulated human exposure to E 171 by feeding mice with E 171-mixed diet and designed 28-day and 84-day exposure experiments to evaluate its potential hepatotoxicity. Conventional toxicological evaluations and global methylation evaluations were further performed. We also performed whole genome bisulfite sequencing (WGBS) of liver DNA from E 171-exposed mice to examine the genome-wide DNA methylation

changes. Our data revealed that E 171 activated ferroptosis through DNA methylation alterations that triggered NCOA4-mediated ferritinophagy, which further induced hepatotoxicity.

Materials and methods

Physicochemical characterization of E 171

E 171 from two different manufacturers were used in this study and designated as E 171-1 and E 171-2. E 171-1 was purchased from Shanghai Jiang Hu Titanium White Product Co., Ltd. (Shanghai, China), and E 171-2 (Product No. 1.00805, Titanium (IV) oxide, Emprove Essential, Ph. Eur., BP, ChP, JP and USP) from Merck KGaA (Darmstadt, Germany, https://www.sigmaaldrich.cn). The particles were visualized under a GeminiSEM 300 scanning electron microscope (ZEISS, Oberkochen, Germany) and a JEM-1200EX transmission electron microscope (JEOL, Tokyo, Japan). The crystal structure was identified using a D8 ADVANCE X-ray powder diffractometry (Bruker, Karlsruhe, Germany).

In addition, 1.2 mg of E 171-1 and E 171-2 powders were each dissolved in 8 mL of anhydrous ethanol. The samples were then vortexed for 10 s and then sonicated using a JY92-II Ultrasonic Processor equipped with a 6 mm probe (Ningbo Scientz Biotechnology Co., Ltd., Ningbo, China) at 40% amplitude for 10 min (1140 J/mL) to achieve sufficient dispersion for analysis [53]. Imaging was performed using a JEM-1200EX transmission electron microscope (JEOL, Tokyo, Japan). The acquired images were counted and analyzed using ImageJ software, following the guidelines proposed by Bresch et al. (rule number 4) [54]. Specifically, the constituent particles of the original E 171 samples were characterized by their minimum and maximum Feret diameter (Fmin and Fmax), mean Feret diameter (Fmean, i.e., the arithmetic mean of Fmin and Fmax), and aspect ratio (Fmax/Fmin).

In vitro digestion of feed with or without E 171

Feed samples with E 171-1, E 171-2, or without E 171 were subjected to in vitro digestion of feed matrices simulating the processes in the human body, and single-particle ICP-MS (spICP-MS) was performed to examine the release of nanosized TiO_2 particles from the food matrix during digestion. Feed samples with 0.32% (3.2 g/kg) of E 171-1 or E 171-2 (same as the feeds for high-dose E 171-1 or E 171-2 group) were prepared and irradiated with Co-60 (Puluteng Biotechnology, Shanghai, China). Artificial saliva, gastric fluid, and intestinal fluid (R22154, R30388, R22156) were purchased from Yuanye Biological Technology (Shanghai, China) for simulating the human digestive environment. Digestion was performed following our previous studies [28]. Briefly, 4.5 g feed samples were mixed with 6 mL artificial saliva and incubated at constant temperature for 5 min (300 rpm, 37 °C). Then, 12 mL gastric juice was added to the feed matrix, and the pH was adjusted to a value of 2. The feed matrix was then incubated for 2 h at 300 rpm and 37 °C. Intestinal juice (12 mL) was subsequently added to the feed matrix, and the pH was adjusted to 6.8. The feed mixture was incubated for 2 h (300 rpm, 37 °C). After each stage, the supernatant was removed, and the samples were immediately diluted with ultrapure water (1:100). They were then filtered through a 5 μm filter [13], and the filtered samples were continued to be diluted to the appropriate concentration (approximately 1:500) for the spICP-MS. Detection of spICP-MS was achieved using an Agilent 8900 Triple Quadrupole ICP-MS instrument (Agilent Technologies, CA, USA) equipped with a microFAST SC injection system. Instrument conditions and method performance are summarized in the Supplementary Material (Table S1).

Animal experiments

Male BALB/c mice weighing 18−22 g (Vital River Laboratory Animal Technologies, Beijing, China) were acclimated for seven days and randomly assigned to the subacute (28-day) or subchronic (84-day) exposure group, housed under a 12-h light/dark cycle at 25 ± 1 °C with a relative humidity of 50 ± 10%. Food and pure water were provided ad libitum. All procedures and experiments on animals were performed under the guidelines of the Animal Care and Use Committee of Zhejiang University School of Medicine and followed the guidelines covered in the Use of Animals in Toxicology.

After the completion of each exposure period, the mice were anesthetized with 1.5% pentobarbital sodium by intraperitoneal injection. The plasma samples from the inferior vena cava were centrifuged at 4000 rpm (4 °C, 10 min). Major organs were removed, including the liver, brain, heart, spleen, lung, and kidney. The weight of each organ was weighed to calculate the organ coefficient (ratio of organ to body weight). The formula was as follows:

$$\text{Organ coefficient} = \frac{\text{organ weight (g)}}{\text{body weight (g)}} \times 100\%$$

Samples were collected and fixed in 10% neutral buffered formalin for further hematoxylin and eosin (H&E) staining. Samples from the lateral liver lobe were taken for WGBS analysis. The rest of the major organs were stored at − 80 °C for subsequent analysis.

Experimental design and feed preparation

Seven experimental groups (eight mice in each group) were designed for subacute and subchronic exposure, respectively, including vehicle control, low-dose E 171-1 (8 mg/kg bw per day), middle-dose E 171-1

(80 mg/kg bw per day), high-dose E 171-1 (320 mg/kg bw per day), low-dose E 171-2 (8 mg/kg bw per day), middle-dose E 171-2 (80 mg/kg bw per day), and high-dose E 171-2 (320 mg/kg bw per day). The dosages for the low-dose (8 mg/kg bw per day) and middle-dose (80 mg/kg bw per day) groups were determined based on the methodology established by the EFSA for assessing the maximum exposure levels to E 171 in adults (18–64 years old) [2]. Specifically, the low and middle doses were approximately equal to the lowest and highest average adult maximum exposure doses (0.6 – 6.8 mg/kg bw per day) [2], respectively, calculated by the conversion of human and mouse body surface area [55]. Since pharmaceuticals, cosmetics, and pigments also contain large amounts of TiO_2, food is only one of the sources of human exposure to TiO_2. The high dose (320 mg/kg bw per day) was four times the middle dose, and all the doses were computed using body surface area normalization. Exposure periods were specified according to the Economic Co-operation and Development Guidelines for rodent oral toxicity studies (Test Guidelines 407 and 408). According to the daily feed intake (0.1 g/g bw per day), the amounts of E 171 added to feed samples were 0.08, 0.8, and 3.2 g/kg, corresponding to the low-, middle-, and high-dose groups, respectively (Table S2). All feeds were prepared by Puluteng Biotechnology and irradiated with Co-60. To incorporate E 171 into animal feed, the E 171 powder was gradually pre-mixed with the feed ingredients in equal amounts until the target percentage of E 171 in the feed was achieved. Subsequently, the pre-mixed feed was further mixed in a high-efficiency mixer (VH-50, Tian He Machinery Equipment, Shanghai, China), during which water, oils, and fats were gradually added.

Sample preparation and scanning transmission electron microscopy (STEM) analysis

Following subchronic treatment, samples obtained from the mouse liver and small intestine were fixed in 2.5% v/v glutaraldehyde overnight. Then, the samples were washed and soaked three times in phosphate buffer (0.1 M, pH 7.0) for 15 min. After dehydrating with graded ethanol (30%, 50%, 70%, 80%, 90%, and 100%) and pure acetone, the samples were treated with a mixture of resin and acetone. The embedded samples were cut using an EM UC7 Ultra-thin microtome (Leica, Wetzlar, Germany) to obtain flakes of 110 – 130 nm, which were collected on nickel or copper grids. The obtained sliced samples were observed by a STEM Nova Nano 450 (Thermo FEI, USA), and the elemental analysis was performed using an EDAX TEAM Octane EDS-70 (Ametek, California, USA) equipped.

Global DNA methylation analysis

Quantification of global DNA was determined by a NanoDrop 2000 (Thermo Fisher Scientific, Waltham, USA) after genomic DNA extraction from the liver using the Wizard Genomic DNA Purification Kit (Promega, Madison, WI, USA). An equal amount of DNA from each sample in each group was well mixed as a testing sample to represent the group. The levels of 5-methylcytosine (5-mC) were detected using a MethylFlash Global DNA Methylation (5-mC) ELISA Easy Kit (EpiGentek, USA), and the 5-hydroxymethylcytosine (5-hmC) levels were detected by a MethylFlash Global DNA Hydroxymethylation (5-hmC) ELISA Easy Kit (EpiGentek).

Whole genome bisulfite sequencing

In the control and E 171-2 middle-dose exposure group, the liver samples from three randomly selected mice were performed for WGBS. As previously described [28], genomic DNA was mixed with lambda DNA and cut into ~ 250 bp fragments by a Covaris S220 Focused-ultra sonicator (Covairs, MA, USA). An EZ DNA Methylation-Gold™ Kit (Zymo Research, USA) was used for bisulfite treatment and KAPA HiFi HotStart Uracil + ReadyMix (2x) was used for PCR amplification. Libraries were sequenced on a HiSeq X Ten (Illumina, USA). Paired-end reads of 150 bp were generated by Shanghai Biotechnology (Shanghai, China).

The quality of sequenced sequences was evaluated using Fastp v 0.20.0 (Fastp, RRID: SCR_016962) and filtered using Trim Galore v 0.4.1 (Trim Galore, RRID: SCR_011847) to obtain clean reads. The main filtering steps were as follows: first, the reads with low overall quality, i.e., Q > 20 in < 50% of the bases, were removed; next, the bases with quality Q < 20 at the 3′ end (base error rate was greater than 0.01) and the splice sequences contained in the reads were removed; finally, sequencing fragments (reads) with lengths less than 70 and unpaired reads were de-selected. Then, using Bismark (v.0.15.0), the genome of the reads after pretreatment was compared using a mouse (mm10) as the reference genome, and possible PCR redundancies were removed.

Quantitative reverse transcription polymerase chain reaction (RT-qPCR) analysis

Total RNA extracted using a RNeasy Mini Kit (Qiagen, Germany) from liver tissue was quantified using the NanoDrop 2000 device, for each group, equivalent amounts of RNA samples from seven mice were taken to prepare the test samples. After reverse transcription with a HiFiScript cDNA Synthesis Kit (CWBIO, Taizhou, China), RT-qPCR was performed using the CFX96 Touch™ Real-Time PCR System (BioRad, CA, USA) with Hieff UNICON® qPCR SYBR Green Master Mix (Yeasen Biotech,

Shanghai, China) and the specific primers (Sangon Biotech, Shanghai, China) shown in Table S3. The housekeeping genes used to normalize the data were *Gapdh* and *Rps29*, and fold changes were calculated using the $2^{-\Delta\Delta Ct}$ method. The experiment was repeated three times.

Western blot analysis

The detailed experimental steps for western blot were described in the previous studies [29]. Briefly, for each group, liver samples from six mice were lysed using a protein lysis buffer, and equal amounts of proteins were mixed as a representative sample. Protein samples were then separated by 10% or 12% sodium dodecyl sulfate–polyacrylamide gel electrophoresis and transferred to polyvinylidene fluoride membranes. The membranes were then blocked in 5% skim milk solution and then incubated overnight at 4 °C with the following primary antibodies: IGF-1 (1:500; Abcam, Cambridge, UK), HSP90B1 (1:1000; Abcam), β-actin (1:1000; Beyotime Biotechnology, Shanghai, China), NCOA4 (1:1000; Abcam), p62 (1:1000; Beyotime Biotechnology), LC3B (1:1000; Beyotime Biotechnology), GAPDH (1:1000; Beyotime Biotechnology), FTH1 (1:1000; Abcam), FTL (1:1000; Abcam), and GPX4 (1:1000; Abcam). The blots were then incubated with horseradish peroxidase-conjugated secondary antibodies (Beyotime Biotechnology). GAPDH or β-actin was used as an internal standard.

Statistical analysis

Values are expressed as mean ± standard deviation (SD). One-way ANOVA followed by Dunnett's test was used to test statistical differences between the E 171-exposed and control groups. Differences with p values < 0.05 were considered statistically significant.

Results

Nanoparticles were present in E 171 and the feed matrix after in vitro digestion

Two types of E 171 (i.e., E 171-1 and E 171-2) were used to assess the potential risk of E 171. E 171-1 is commonly used as a food additive in mainland China (Jiang Hu Titanium White, Shanghai, China), while E 171-2 is widely used in food and pharmaceuticals worldwide (Merck KGaA, Darmstadt, Germany). The physicochemical properties of nanoparticles determine their uptake and potential hazards when they enter in vivo [56]. Thus, the physicochemical properties of the two types of E 171 were first characterized. As shown in Fig. 1A, both materials exhibited an approximately spherical shape and contained nanoparticles detected by scanning electron microscopy (SEM) and transmission electron microscopy (TEM), while large agglomerates were also observed. X-ray powder diffractometry (XRD) showed that both types of E 171 are anatase, which is a common type of TiO_2 crystals used in food products (Fig. 1B) [57].

Table 1 further summarizes the results obtained by analyzing E 171-1 (n = 477) and E 171-2 (n = 531) particles using TEM. The average Fmin of E 171-1 and E 171-2 was 111.8 nm and 123.9 nm, respectively. E 171-1 and E 171-2 contain 40.5% and 33.9% of particles with Fmin less than 100 nm, respectively (in terms of number share). In terms of particle distribution, the sizes of both E 171 particles were mainly distributed between 40 and 250 nm, and the Fmean diameter of the constituent nanoparticles is generally around 90 nm (Fig. 1C).

The colloidal properties of the two types of E 171 samples in ddH_2O or in simulated human digestive juice were determined by dynamic light scattering (DLS). As shown in Table S4, the hydrodynamic diameter (d_H) of E 171-1 in ddH_2O was smaller than that of E 171-2 (282.8 ± 6.9 nm versus 543.8 ± 25.4 nm). In artificial saliva, the d_H of E 171-1 and E 171-2 were similar to each other, at 1022.2 ± 10.4 nm and 975.6 ± 63.7 nm, respectively. The d_H of E 171-1 in artificial gastric fluid was similar to that in artificial intestinal fluid (591.4 ± 10.6 nm and 587.2 ± 13.0 nm). In contrast, the d_H of E 171-2 in artificial gastric fluid was greater than that in artificial intestinal fluid (940.9 ± 39.3 nm and 680.4 ± 2.4 nm, respectively). The d_H of E 171 in artificial saliva is greater than that in artificial gastric and intestinal fluid, possibly because of the neutral pH (pH = 7) of the artificial saliva. Previous studies have demonstrated that calcium and phosphate in the digestive fluid precipitate on the surface of E 171, thereby increasing its d_H at pH ≥ 7 [58]. Furthermore, in agreement with previous studies [59], E 171 showed a smaller d_H in artificial intestinal fluids in this study.

The ζ potentials determined via electrophoretic light scattering (ELS) of E 171-1 and E 171-2 were negative in ddH_2O (−11.8 ± 0.9 mV and −13.7 ± 0.9 mV), artificial saliva (−13.0 ± 0.5 mV and −13.8 ± 0.7 mV), and artificial intestinal fluid (−29.5 ± 1.8 mV and −19.6 ± 0.9 mV). In contrast, the ζ potential of E 171-1 and E 171-2 became positive in the acidic artificial gastric fluid (15.6 ± 0.7 mV and 14.4 ± 0.6 mV). Similarly, previous studies showed that the iso-electric point pH of E 171 was at approximately 3.3, and E 171 carried a negative surface charge at higher pH (pH ≥ 4) [60].

E 171-containing foods may release TiO_2 nanoparticles during digestion, which may influence their toxicity in vivo. Thus, three types of feed samples were analyzed to evaluate the effects of simulated human digestion on E 171 in food: normal feed samples, normal feed samples with E 171-1, and normal feed samples with E 171-2. These feed samples were sequentially digested using saliva juice, gastric juice, and intestinal juice to simulate the human

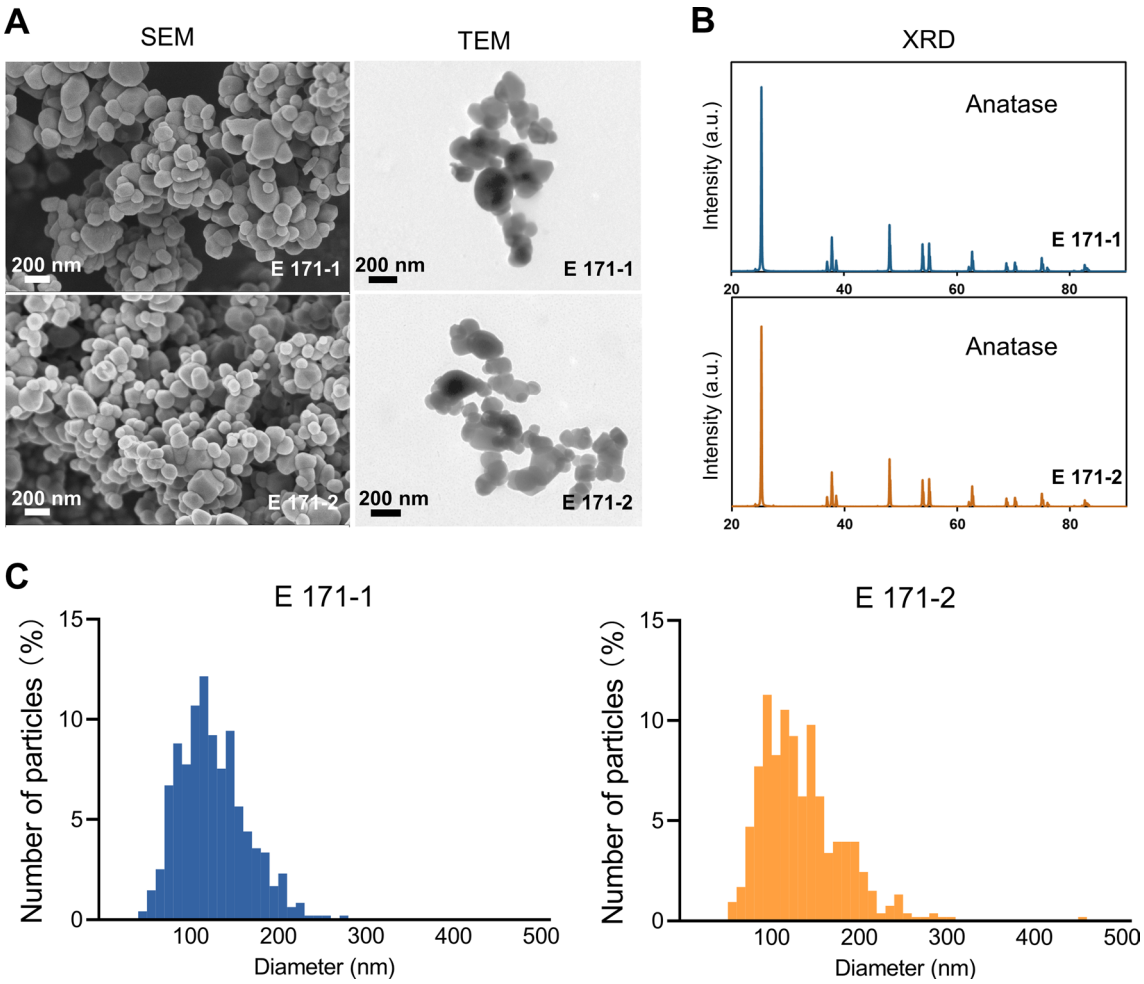

Fig. 1 Physicochemical properties of E 171. (**A**) Characterization of E 171-1 and E 171-2 using TEM and SEM. The scale bar is 200 nm. (**B**) Crystal structure of E 171-1 and E 171-2 by XRD. (**C**) E 171 number-based particle size distributions (PSDs) of Fmean determined by TEM

Table 1 Summary of the number-based PSDs of E 171-1 ($n=477$) and E 171-2 ($n=531$) as determined by TEM: median and mean values of the Fmin, Fmax, and aspect ratio; number-based percentages of particles with a Fmin smaller than 100 nm and 250 nm

TiO_2	Fmin		Fmax		Aspect ratio		% of constituent Particles with Fmin	
	Median (nm)	Mean (nm)	Median (nm)	Mean (nm)	Median	Mean	< 100 nm	< 250 nm
E 171-1	107.5	111.8	131.7	138.2	1.2	1.2	40.5	100.0
E 171-2	116.7	123.9	133.1	143.4	1.1	1.2	33.9	99.2

digestive processes in vivo. The spICP-MS was used to detect the PSDs of E 171, incorporating samples after ultrasound treatment or simulated human gastrointestinal tract digestion. The spICP-MS was first performed on TiO_2-P25 (Merck KGaA, Darmstadt, Germany), which, according to the supplier, had an initial particle size of 21 nm (TEM). The results showed that the average size of TiO_2-P25 dispersed in ultrapure water was 57.3 ± 4.0 nm ($n=3$, Fig. S1), which was in agreement with the results of spICP-MS performed in a previous study using a NexION 350 ICP-MS on TiO_2-P25 from the same supplier [61]. For E 171-1 and E 171-2 dispersed in ultrapure water, spICP-MS determination of the PSDs of TiO_2 particles showed that the most predominant distribution of particles in both E 171 samples was between 90 and 150 nm (Fig. 2A). The percentage of TiO_2 particles smaller than 100 nm was 17% and 10% for

both E 171 samples, respectively (Table S5). Next, spICP-MS was performed on TiO_2 particles released from normal feed or feed containing E 171 that had been digested sequentially with artificial saliva, artificial gastric fluid, and artificial intestinal fluid. No TiO_2 particles were detected at any stage of digestion of normal feed, while TiO_2 particles were detected at all stages of digestion of feed containing E 171-1 or E 171-2. The spICP-MS results showed that the TiO_2 particles detected after salivary and gastric digestion were larger than those detected in E 171 dispersed in ultrapure water after sonication, with no particles smaller than 100 nm detected (Fig. 2B). Notably, after the final artificial intestinal fluid digestion, the TiO_2 particles released from feeds containing E 171 were significantly smaller in

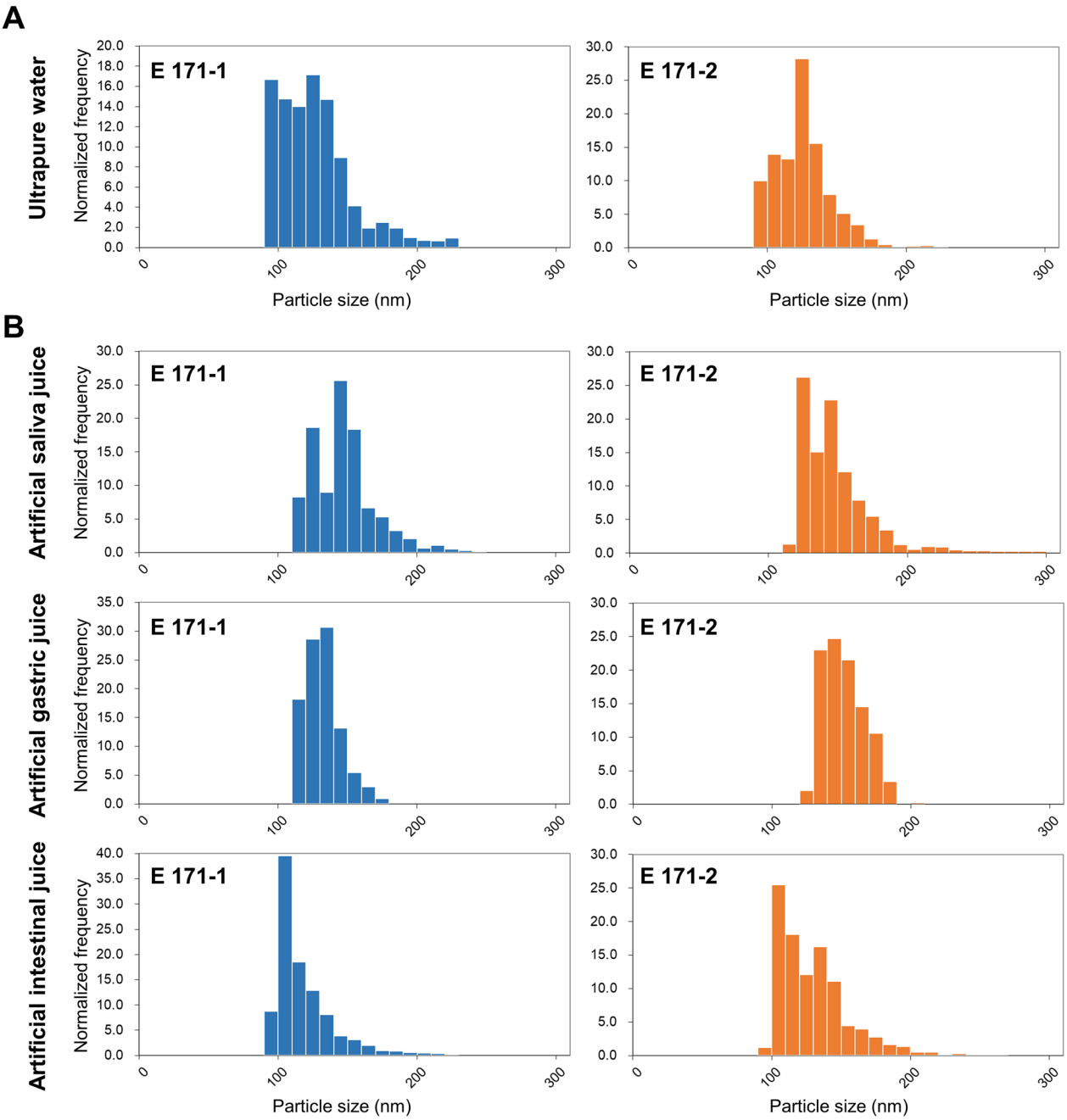

Fig. 2 Number-based PSDs of TiO_2 particles determined by spICP-MS. (**A**) The PSDs of TiO_2 particles of E 171-1 and E 171-2 dispersed in ultrapure water. (**B**) The PSDs of TiO_2 particles of feed samples containing E 171-1 or E 171-2 after successive digestion with artificial saliva juice, artificial gastric juice, and artificial intestinal juice

size than those released by the artificial saliva and gastric fluid digestion stages (Fig. 2B). During the artificial intestinal fluid digestion stage, the percentage of TiO_2 particles smaller than 100 nm in the particles released from feeds containing E 171-1 or E 171-2 was 10% and 1%, respectively (Table S5).

Effects of subacute and subchronic exposure of E 171 on mice

Mice were exposed to E 171 for 28 or 84 days to examine the phenotypic changes induced by subacute and subchronic oral exposure. Conventional toxicological indicators were evaluated in mice after subacute and subchronic exposure to E 171-1 and E 171-2. The low- and middle-dose (8 mg/kg bw per day and 80 mg/kg bw per day) E 171 groups were designed based on the maximum human exposure level (0.6 − 6.8 mg/kg bw per day for adults aged 18 − 64) reported by the EFSA [2], calculated by the conversion of human and mouse body surface area [55]. The high-dose (320 mg/kg bw per day) E 171 groups were used to evaluate the potential risk of E 171 in higher exposure situations. The actual oral exposure doses of TiO_2 were calculated using the average daily feed intake of the mice and the TiO_2 content of the feed samples (Fig. S2, Table S2). The results confirmed that the actual doses matched the planned doses (Table S2).

No significant changes were observed in the body weights of mice after subacute or subchronic treatment with any of the three doses of E 171-1 or E 171-2, compared with the control group (Figs. 3A and S3). However, the liver coefficients (ratio of liver to body weight) of mice exposed to the high dose of E 171-2 for 84 days decreased significantly (Fig. 3B). No other organ coefficients changed significantly after exposure to E 171 (Figs. S4A and S5). Similarly, a previous study also reported reduced liver coefficients in C57BL/6 mice after 16 weeks of E 171 administration via drinking water at 5 mg/kg [17]. These results suggested that oral exposure to E 171 may have detrimental effects on the liver.

To further evaluate the liver injury caused by oral exposure to E 171, plasma alanine transaminase (ALT) and aspartate transaminase (AST) levels were measured. Triglycerides (TG), total cholesterol (TC), and total bilirubin (TBIL) in plasma were measured to assess lipid metabolism changes. After 28 days of exposure to E 171-1 or E 171-2, none of the three dose groups showed significant changes in any of these parameters compared with the control group (Fig. S4B). However, high-dose E 171 exposure for 84 days increased ALT and AST levels, especially in the high-dose E 171-1 group (Fig. 3C). Meanwhile, TG levels in plasma were significantly reduced in the high-dose E 171-1 group and both TBIL and TG levels in plasma were significantly reduced in the high-dose E 171-2 group after 84 days of exposure to E 171 (Fig. 3D). These results indicated that subchronic exposure to high doses of E 171 can induce mild liver injury and lipid metabolism alterations. A previous study reported a similar phenomenon in CD1 mice after intravenous injection of E 171 (6 mg/kg bw per day), which elevated ALT and AST levels above the reference values after 24 and 96 h [31].

Liver samples from mice exposed to E 171-1 and E 171-2 for 28 and 84 days were subjected to H&E staining. The liver of mice exposed for 28 days showed no significant changes (Fig. S6). However, inflammatory cell infiltration was found in the liver tissues of mice exposed to all three E 171-1 and E 171-2 doses for 84 days (Fig. 3E). These results indicated that two types of E 171, which contain a fraction of nanoscale TiO_2 particles, can induce hepatotoxicity in mice.

Digestion and distribution of E 171 in vivo

To determine whether E 171 can accumulate in the liver of mice at both low and high doses when administered orally, the small intestine and liver of mice exposed to low- and high-dose E 171 for 84 days were examined using STEM and energy dispersive X-ray spectroscopy (EDS). As shown in Fig. 4A, after 84-day exposure to E 171, TiO_2 particles were found in the small intestine of mice in the low- and high-dose E 171-1 and E 171-2 groups. The particles appeared individually or in aggregates in the microvilli and enterocytes with an average size of approximately 100 nm. Furthermore, EDS analysis showed that the single particles and aggregates were made of TiO_2 (Fig. S7A). Importantly, STEM further revealed the presence of single particles and aggregates in liver sections after 84-day exposure to E 171-1 or E 171-2 (Fig. 4B), and EDS confirmed that the particles were made of TiO_2 (Fig. S7B). Moreover, we detected TiO_2 aggregates in the hepatic vessel of mice in the high-dose E 171-2 group (Fig. 4B), implying that they reached the liver via blood circulation.

(See figure on next page.)

Fig. 3 Conventional toxicological evaluation of the effects on mice exposed to E 171 for 84 days. (**A**) Body weight, (**B**) Liver coefficients, (**C**) Plasma ALT and AST levels, and (**D**) Plasma TBIL, TG and TC levels, $n = 8$. (**E**) Representative H&E staining plots of liver, $n = 4$. *n* indicates the number of mice in each group. Significance is indicated as $^*p < 0.05$ and $^{**}p < 0.01$, compared with the control group

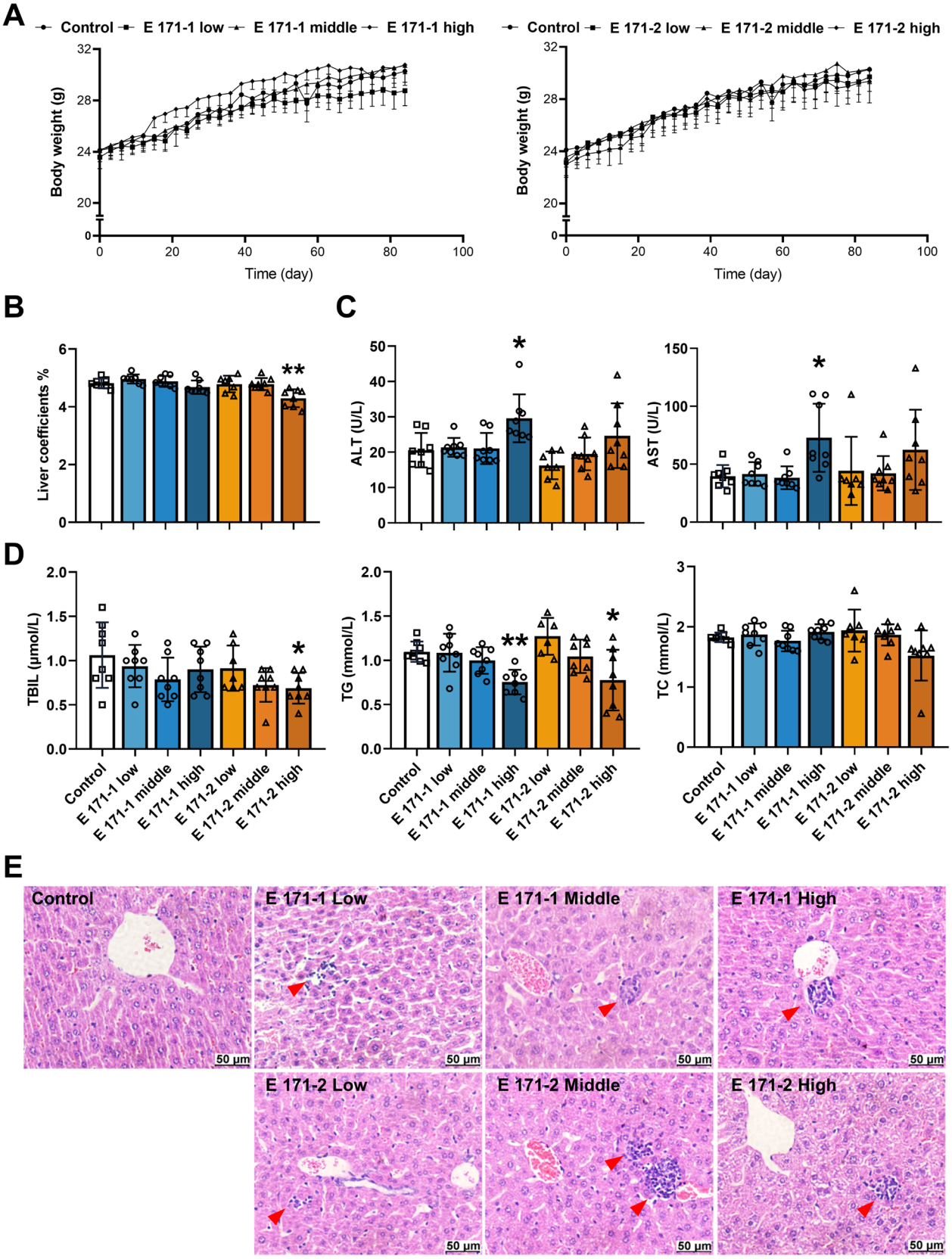

Fig. 3 (See legend on previous page.)

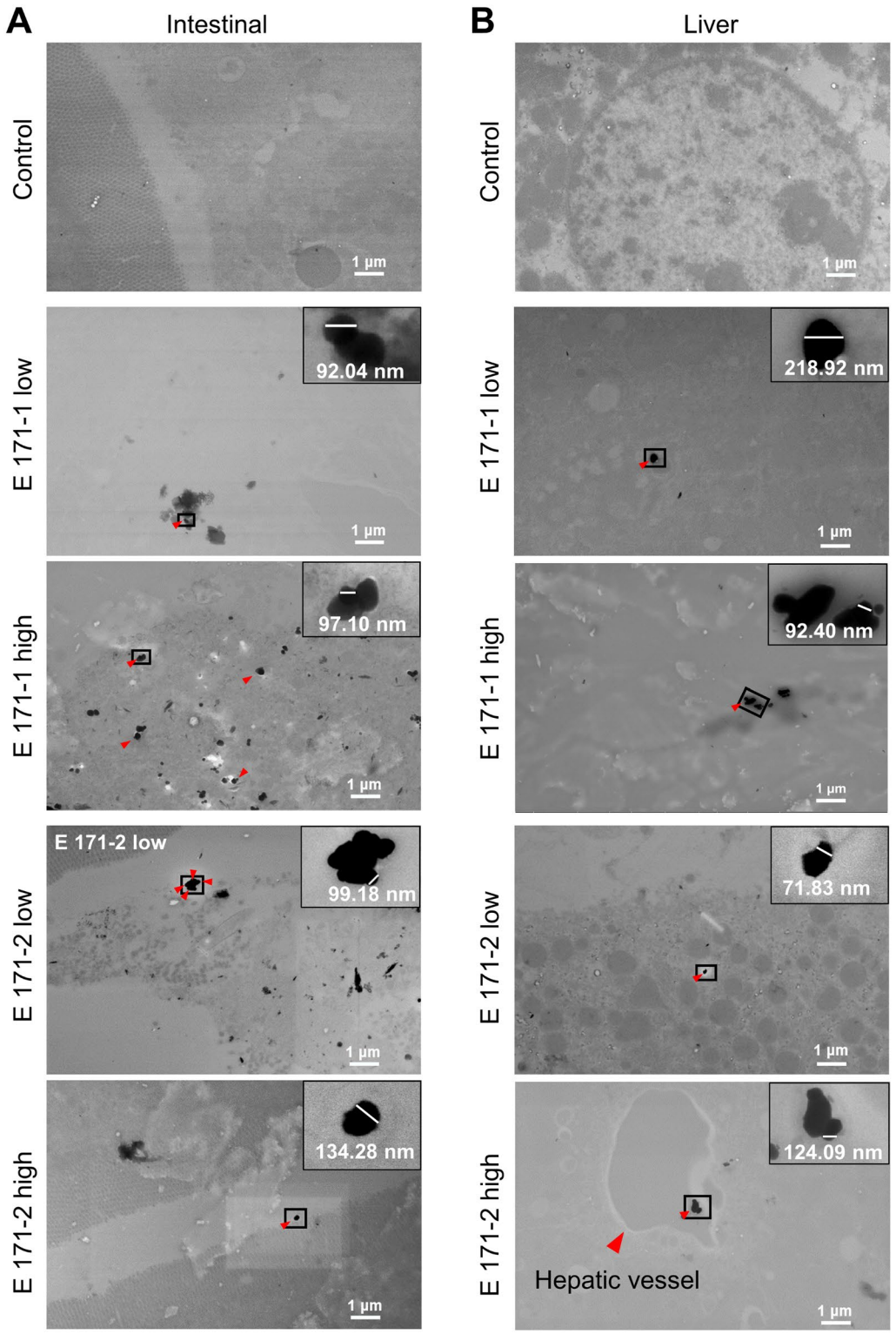

Fig. 4 STEM images of the small intestine and liver. Representative STEM images of the small intestine (**A**) and liver (**B**) of mice after 84 days of E 171-1 or E 171-2 exposure. TiO_2 particles or aggregates (red arrows) were observed near the small intestinal villi, within the enterocytes, and in the liver. A magnification of 10,000 × was used. High means high-dose E 171-exposed group, and low indicates low-dose E 171-exposed group

Effects of E 171 exposure on DNA methylation and its elements in the liver

DNA methylation and hydroxymethylation levels may be significantly altered after dietary exposure to nanoparticles [28]. Thus, the changes in global DNA methylation and hydroxymethylation levels were assessed in vivo by comparing the 5-mC and 5-hmC levels in the liver samples of the E 171-exposed and control mice. A slight decrease in 5-mC levels was found in the liver of mice in all three doses of E 171 exposure for 28 days, especially in the low- and high-dose E 171-1 groups as well as the middle- and high-dose E 171-2 groups, compared with the control group (Fig. 5A). A similar trend was observed in liver tissue with 84-day E 171 treatment (Fig. 5B): exposure to three doses of E 171-2 resulted in a significant and dose-dependent decrease in hepatic 5-mC levels, and the high-dose E 171-1 group also showed a significant reduction in 5-mC levels compared with the control group. Hepatic 5-hmC levels did not change significantly after 28-day treatment with E 171-1 or E 171-2 (Fig. 5C). However, there was a significant reduction in liver 5-hmC levels after high-dose E 171-1 exposure and middle- and high-dose E 171-2 exposure for 84 days (Fig. 5D).

We further explored the expression changes of methylation elements linked to 5-mC and 5-hmC levels in liver exposure to E 171 for 28 and 84 days, including DNA methyltransferases and the TET family. The expression levels of *Dnmt1, Dnmt3a, Tet2,* and *Tet3* showed no significant change in the liver of mice exposed to any of the three doses of E 171-1 or E 171-2 for 28 days. By contrast, *Dnmt1* expression was slightly decreased in the liver of mice exposed to all three doses of E 171 for 84 days, and significantly downregulated ($\geq$1.5-fold) exposed to the middle-dose E 171-1 as well as the middle- and high-dose E 171-2 (Fig. 5E). Thus, lower hepatic 5-mC levels after subchronic exposure to E 171 may be due to the downregulation of *Dnmt1*. Furthermore, the expression of *Tet2* and *Tet3* in liver tissue was significantly downregulated after exposure to E 171 for 84 days (Fig. 5F, G), which was consistent with the decrease in 5-hmC levels. The decrease in the levels of 5-mC and 5-hmC indicated that E 171 exposure affects DNA methylation and demethylation in the liver. Exposure to engineered and food-grade nanomaterials has been reported to deregulate transposable factor expression [28, 62]. Therefore, we further evaluated the changes in transposable factor expression after 28-day and 84-day exposure to E 171. The expression of *LINE-1 ORF1, LINE-1 ORF2, SINEB1*, or *SINEB2* in liver tissue did not significantly change after exposure to E 171 for 28 days in all groups, but exposure to all doses of E 171-1 or E 171-2 for 84 days upregulated *LINE-1 ORF1* and *LINE-1 ORF2* expression in liver tissue (Figs. 5H and S8).

Our findings suggested that exposure to E 171 for 84 days results in changes in global DNA methylation and hydroxymethylation in the liver of mice. Moreover, the levels of 5-mC and 5-hmC significantly changed in the liver after E 171 treatment for 28 days, but not the organ coefficients, blood biochemical indices, or histopathological patterns. These results suggested that global DNA methylation and hydroxymethylation are sensitive indicators of E 171 toxicity.

DNA methylation landscape

The livers of mice in the middle-dose E 171-2 group were selected for further DNA methylation analysis for the following reasons: (1) E 171-2 is a common food and pharmaceutical additive; (2) The exposure level of the middle-dose E 171-2 group (80 mg/kg bw per day) was within the maximum human exposure level (0.6–6.8 mg/kg bw per day), calculated by the conversion of human and mouse body surface area [55]; (3) The liver of the mice in the middle-dose E 171-2 group exhibited significant pathological and DNA methylation changes similar to those of the high-dose E 171-2 group. We performed WGBS on the liver of mice exposed to the middle dose of E 171-2 to investigate the mechanisms underlying the changes in DNA methylation induced by E 171 exposure. Table S6 shows the quality and clean reads of the raw sequencing data after WGBS. Based on the WGBS results, each sample had a basic quality of Q20 > 93%. The alignment of mouse genome sequences revealed a unique alignment rate of over 69% and a conversion efficiency exceeding 99.5% for each sample. Therefore, the samples met the quality criteria for subsequent analysis. Based on the methylation level of CpG sites for each liver sample, principal component analysis was used to assess similarities and dissimilarities between samples. The samples from the control and middle-dose E 171-2 groups showed clear distinctions, indicating significant methylation changes in the livers of mice treated with middle-dose E 171-2 for 84 days (Fig. S9).

In addition, the DNA methylation levels in mCG, mCHG, and mCHH contexts in the liver were analyzed and visually represented by chromosome-based Circos plots. The changes of methylation in the mCG, mCHG, and mCHH environments were observed in the liver of mice in the middle-dose E 171-2 group compared with the control group (Fig. 6A–C). Several methylation alterations were observed after exposure to E 171 for 84 days. Hypomethylation in the mCG sites in several regions was detected, including 65 – 70 Mb in the Y chromosome, 40–45 Mb in chromosome 1, 130–135 Mb in chromosome 7, and 10–15 Mb in chromosome 18 (Fig. 6A). While in the liver mCHG sites, several hypomethylation regions were detected,

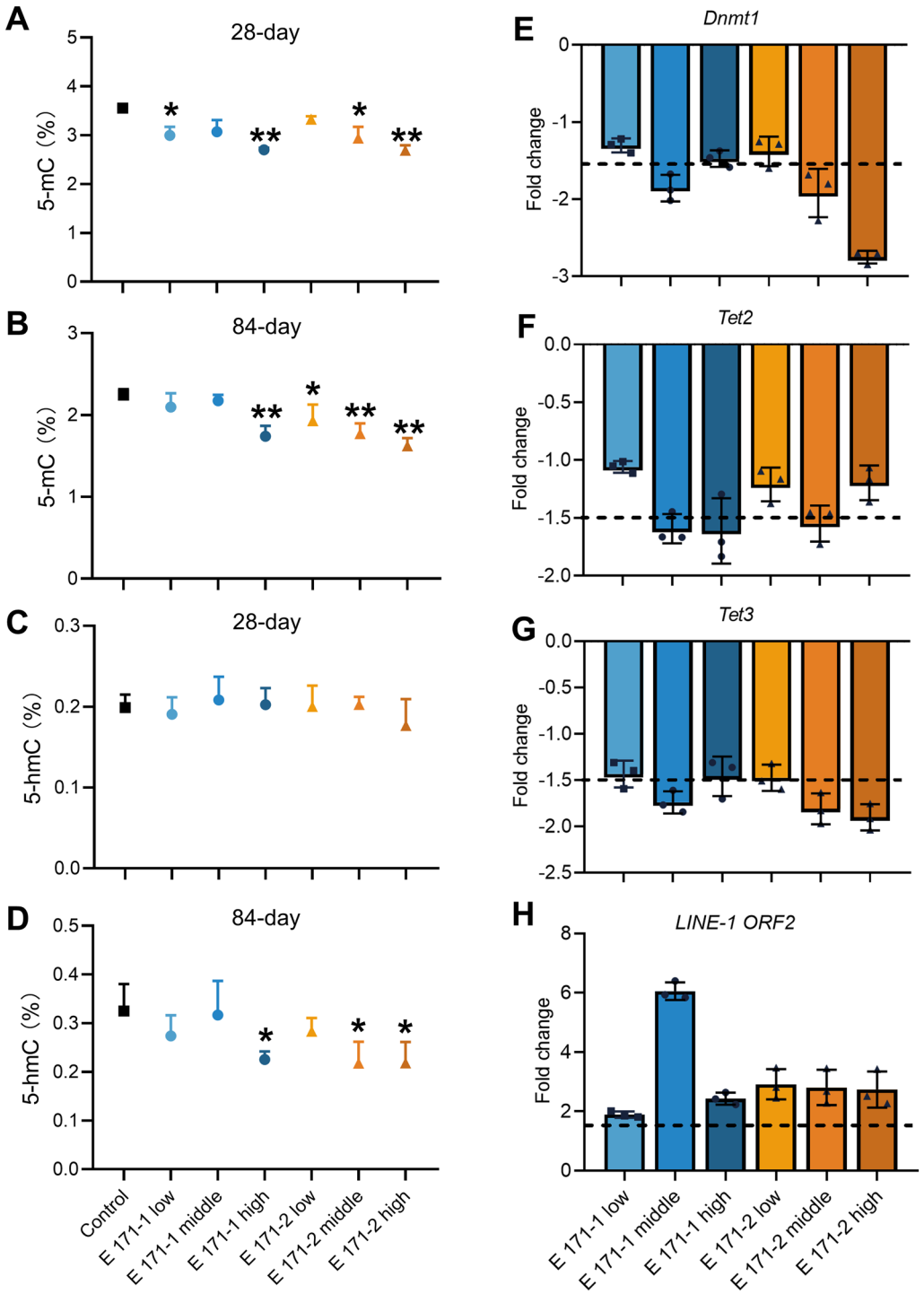

Fig. 5 Global DNA methylation and hydroxymethylation changes in the liver of mice exposed to E 171. (**A**, **B**) The levels of 5-mC in the liver tissue of mice treated with E 171 for 28 (**A**) and 84 days (**B**), $n = 7$. (**C**, **D**) The levels of 5-hmC in the liver tissue of mice treated with E 171 for 28 (**C**) and 84 days (**D**), $n = 7$. (**E**–**H**) Expression levels of *Dnmt1* (**E**), *Tet2* (**F**), *Tet3* (**G**), and *LINE-1 ORF2* (**H**) in the liver of mice treated with E 171 for 84 days, $n = 7$. *n* indicates the number of mice in each group. Statistical significance is indicated as $^{*}p < 0.05$ and $^{**}p < 0.01$, compared with the control group

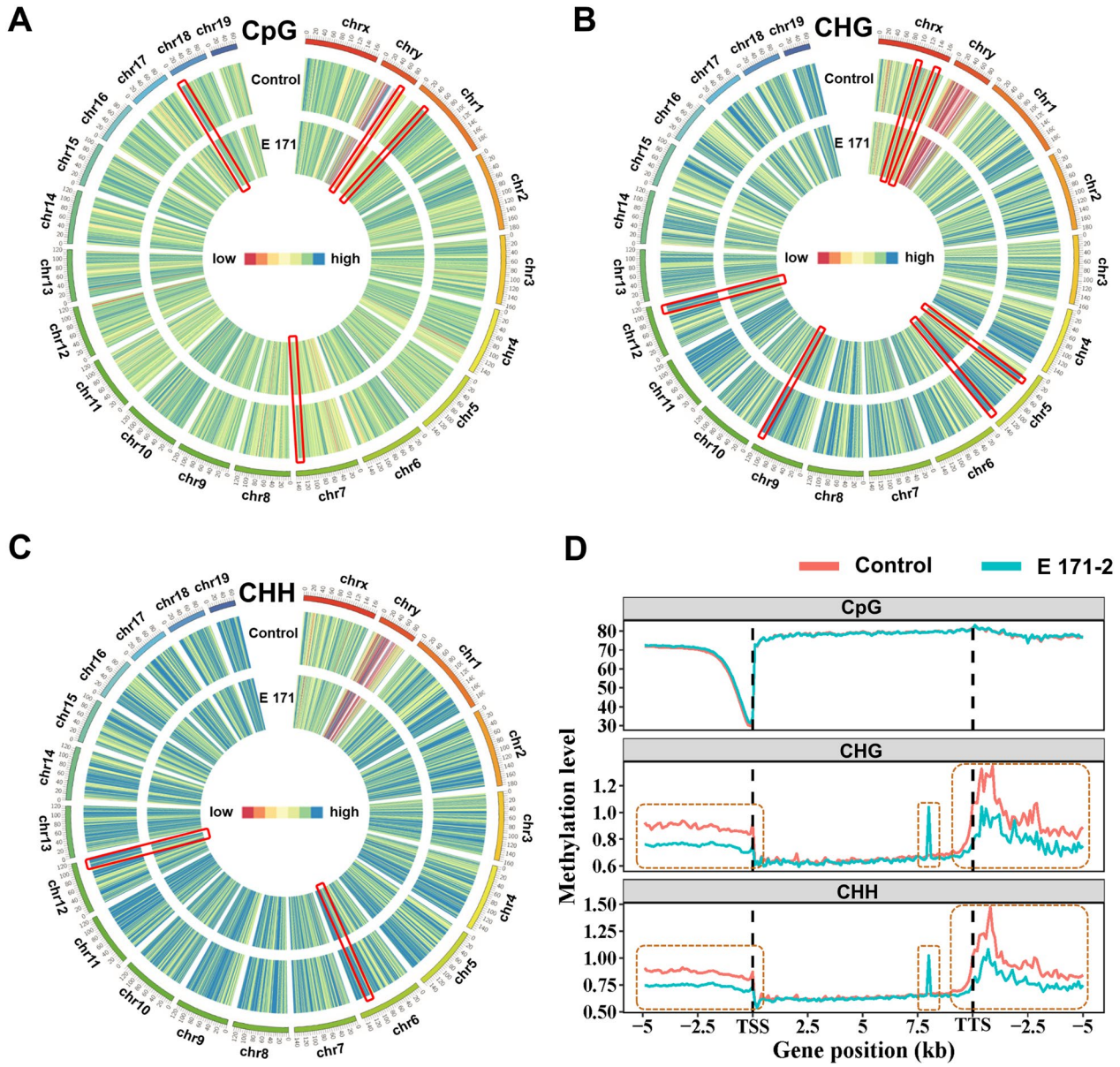

Fig. 6 Genomic DNA methylation landscape in the liver. (**A**–**C**) Circos plots of mCpG (**A**), mCHG (**B**), and mCHH (**C**) methylation levels in 21 chromosomes from liver tissue. Hypomethylation regions are shown in the red boxes. (**D**) Distribution of DNA methylation alterations in different regions in liver tissue

such as 100–105 Mb and 150–155 Mb in chromosome X, 30–35 Mb and 130–140 Mb in chromosome 5, 115–120 Mb in chromosome 9, 100–105 Mb and 110–120 Mb in chromosome 12 (Fig. 6B). In the liver mCHH sites, 115–120 Mb in chromosome 6, 100–105 Mb, and 110–120 Mb in chromosome 12 were hypomethylated (Fig. 6C). In addition, a slight increase in upstream and transcription start sites (TSS) regions of the mCG sites was observed in the liver of mice treated with middle-dose E 171-2 for 84 days. In the mCHG and mCHH sites, E 171 treatment showed a marked methylation decrease in the upstream, TSS, transcription termination sites (TES), and downstream regions (Fig. 6D). Notably, E 171 induced elevated methylation levels in the region near the 8 kb position of the gene body in both mCHG and mCHH environments in the livers of mice exposed to middle-dose E 171-2 for 84 days.

Differentially methylated sites, regions, and genes after exposure to E 171

Differentially methylated sites (DMSs) were identified using the Dispersion Shrinkage for Sequencing data (DSS) tool with parameters "p value ≤ 0.05 and methylation difference degree > 10%." The methylation variation patterns in the liver that resulted from subchronic exposure to E 171 were assessed by selecting the DMSs and visualizing the clustered heat maps (Fig. S10). To further investigate DNA methylation alterations in different regions after E 171 exposure, we screened the differentially methylated regions (DMRs) using the DSS (call DMR) following parameters "p value ≤ 0.05" and "at least 3 nCG." A total of 1409 DMRs were detected in the mCG sites of the liver tissue. Further analysis revealed that the distribution of DMRs varied in different gene regions. In the mCG sites of the liver, DMRs were primarily located in intron and intergenic regions, followed by promoter regions and exons. In the mCHG and mCHH environments, DMRs were mostly located in intergenic regions and, to a lesser extent, in the introns (Fig. 7A).

Notably, the DMR number detected in the mCHG and mCHH environments (4911 DMRs and 12,070 DMRs, respectively) was significantly larger than those in the mCG environments (1409 DMRs), including in the promoter regions that regulate gene expression (Fig. 7A) [63]. Thus, exposure to E 171 may cause more changes in the mCHG and mCHH environments than mCG environments in the liver tissue.

E 171 may cause lipid metabolism changes in the liver

The biological functions of differentially methylated genes (DMGs) in liver tissue were further investigated based on the Gene Ontology Biological Processes (GO) and Kyoto Encyclopedia of Genes and Genomes (KEGG) database. After subchronic exposure to E 171, the insulin metabolic process pathway was significantly enriched (Fig. 7B). Insulin metabolism, which occurs mainly in the liver, affects both physiological processes like fat formation and disease development [64, 65]. The involvement of insulin metabolism and the reduced TBIL and TG plasma levels indicate that subchronic exposure to E 171 may cause changes in hepatic lipid metabolism. To examine the insulin metabolic process pathway, we analyzed the genes with significant changes and observed substantial hypomethylation in the promoter regions of the key genes *Igf-1* and *Hsp90b1*. The results showed that the protein expression levels of IGF-1 and HSP90B1 in the liver of mice were significantly upregulated after 84 days of exposure to E 171, especially exposure to middle-dose E 171-2 (Fig. 7D). IGF-1, which is similar to insulin, regulates glucose metabolism and is associated with lipid levels in the liver [66–68], and HSP90B1 can inhibit high glucose-induced insulin secretion [69]. These findings implied that exposure to E 171 may alter the metabolism and, subsequently, the levels of hepatic lipids.

E 171 triggered ferroptosis via NCOA4-mediated ferritinophagy in the liver

KEGG pathway analysis of DMGs showed that the ferroptosis pathway was also significantly enriched (Fig. 7C). To explore the role of DNA methylation regulation in E 171-induced potential ferroptosis, we examined the DNA methylation profiles of *Ncoa4*, *Sqstm1*, and *Map1lc3b*, the key genes encoding NCOA4, p62, and LC3B proteins that modulate ferroptosis via ferritinophagy, in the liver of mice exposed to middle-dose E 171-2 for 84 days. After 84 days of E 171 exposure, the methylation levels of the promoter regions of *Ncoa4* in mCHG and mCHH contexts in mouse liver were significantly lower than those of the control group (Fig. 8A). The 84-day exposure to E 171 also resulted in reduced DNA methylation levels at multiple sites within the promoter regions of *Sqstm1* and *Map1lc3b* in the liver, which were observed in the mCpG, mCHG, and mCHH contexts (Fig. 8B, C). We further analyzed the protein expression of NCOA4, p62, and LC3B in the liver of mice after 84 days of exposure to E 171. The results showed that the protein expression levels of NCOA4 were significantly elevated in a dose-dependent way in the livers of mice exposed to E 171 for 84 days. In addition, both p62 and LC3II (a conjugated form of LC3B) were significantly elevated in the livers of mice exposed to E 171, especially in the middle- and high-dose E 171-2 groups, compared with the control group (Fig. 8E). These results indicated that E 171 might upregulate the expression of *Ncoa4*, *Sqstm1*, and *Map1lc3b* by decreasing their promoter methylation levels, resulting in higher levels of NCOA4, p62, and LC3B expression in mouse liver and affecting NCOA4-mediated ferritinophagy.

Since NCOA4-mediated ferritinophagy plays a crucial role in the regulation of ferroptosis, we further assessed the expressions of the key proteins involved in ferroptosis. The results showed that the protein expression levels of both FTH1 and FTL were significantly decreased in the livers of mice exposed to E 171, especially in the high-dose E 171-1 group and the middle- and high-dose E 171-2 groups, compared with the control group (Fig. 8F). In addition, exposure to E 171 induced a significant dose-dependent decrease of the protein expression level of GPX4 in mouse liver in the middle- and high-dose groups. Reduced protein expression levels of FTH1, FTL, and GPX4 in the livers of E 171-treated mice may greatly contribute to the accumulation of lipid peroxidation thereby triggering ferroptosis.

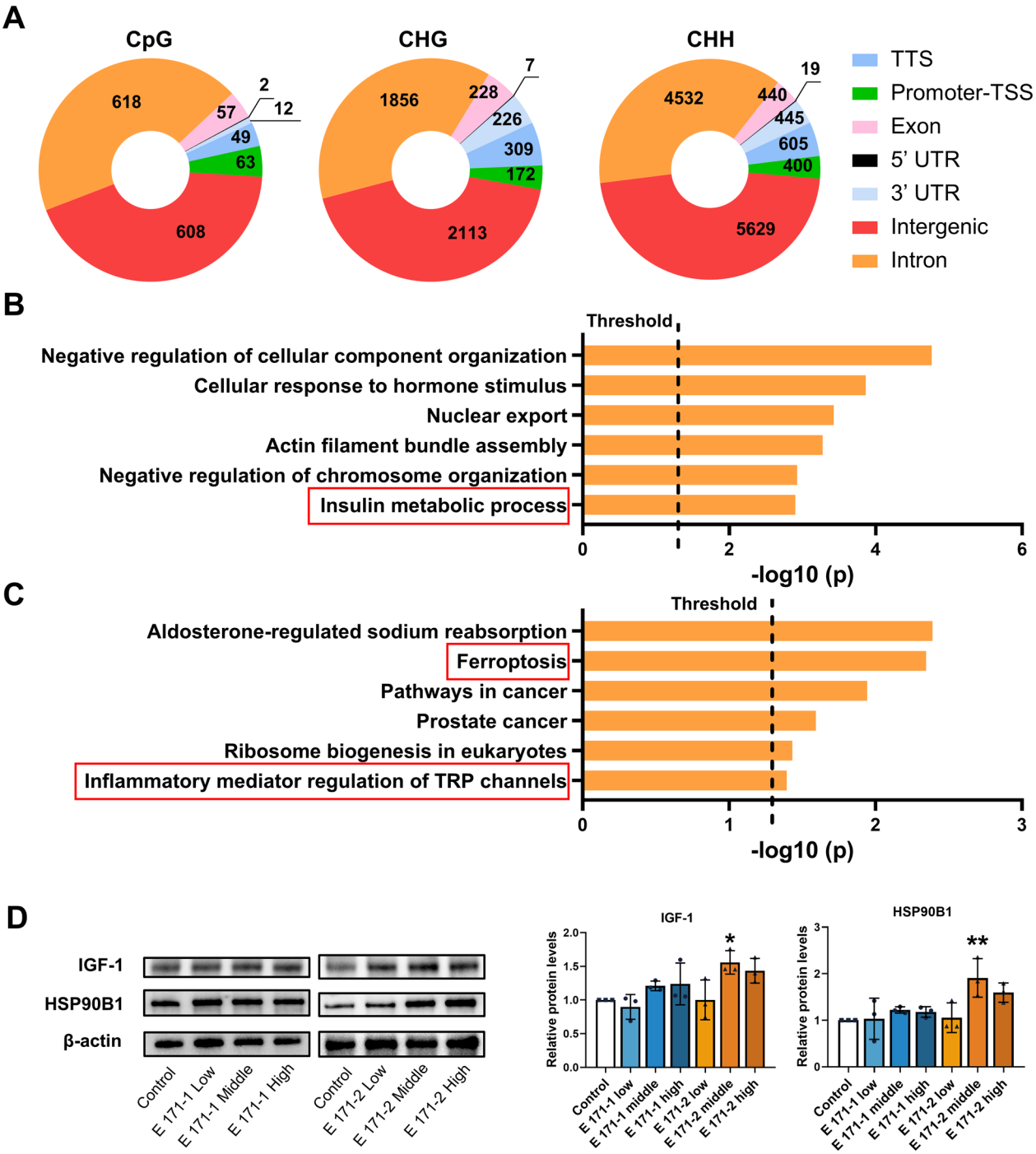

Fig. 7 DMRs and DMGs in the liver. (**A**) Distribution and proportion of DMRs corresponding to mCpG, mCHG, and mCHH sites in liver tissue. (**B**, **C**) Pathway enrichment analysis based on GO (**B**) and KEGG database (**C**). (**D**) Changes in protein expression of IGF-1 and HSP90B1 in the liver, $n = 6$. n indicates the number of mice in each group. Statistical significance is indicated as $^{*}p < 0.05$ and $^{**}p < 0.01$, compared with the control group

Discussion

E 171 has been confirmed to enter the blood circulation of human volunteers through oral exposure [14] and may accumulate in the liver [30–32]. Here, our study shows for the first time that long-term oral exposure to human-relevant doses of E 171 within a food matrix may pose a liver risk through DNA methylation alterations in mice. We show that E 171 when incorporated

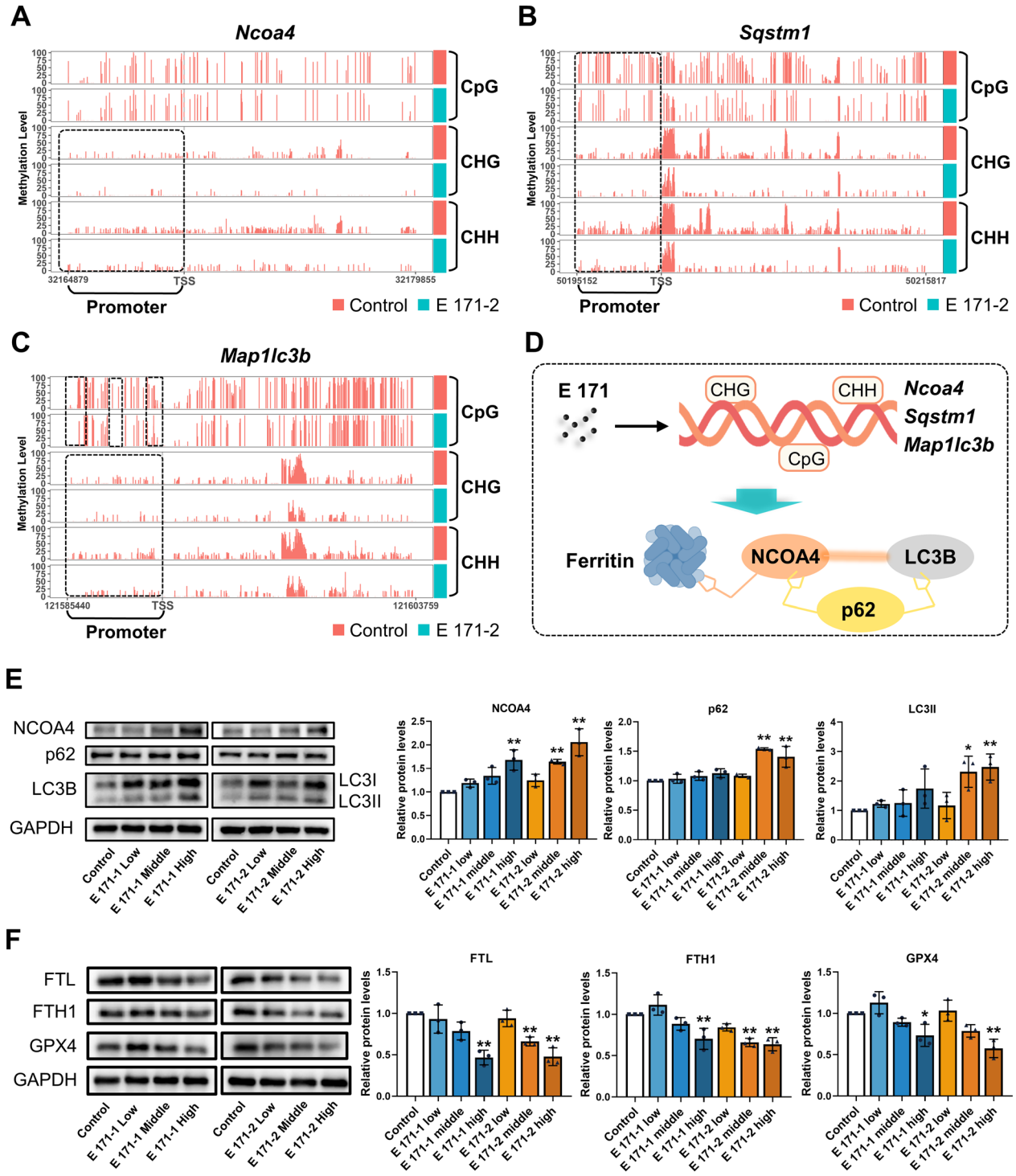

Fig. 8 Effects of E 171 treatment on DNA methylation and protein expression in mouse liver. (**A**–**C**) DNA methylation profiles of *Ncoa4* (**A**), *Sqstm1* (**B**), and *Map1lc3b* (**C**) in mCpG, mCHG, and mCHH environments. (**D**) Schematic diagram of E 171 promoting the process of ferritinophagy by affecting DNA methylation. (**E**) Changes in protein expression of NCOA4, p62, and LC3II in the liver, $n = 6$. (**F**) Changes in protein expression of FTL, FTH1, and GPX4 in the liver, $n = 6$. *n* indicates the number of mice in each group. Statistical significance is indicated as $^{*}p < 0.05$ and $^{**}p < 0.01$, compared with the control group

into a food matrix, released nanoparticles during intestinal digestion. Following 28 days of oral exposure to E 171 within the maximum human exposure levels, E 171 elicited notable DNA methylation changes in the liver of mice without inducing significant pathological alterations. After 84-day exposure to human-relevant doses of E 171, the TiO_2 particles accumulated in the liver of mice via intestinal absorption, leading to liver damage and inflammatory responses. Furthermore, exposure to E 171 for 84 days elicited dose-dependent DNA methylation alterations in the mouse liver, as well as causing significant DNA methylation changes in both CG and non-CG contexts. Our findings show that E 171-induced DNA methylation changes prompt ferroptosis through NCOA4-mediated ferritinophagy, a critical mechanism behind E 171-related liver injury.

This study demonstrates that the intestinal digestion stage is crucial for the breakdown of E 171 mixed in the food matrix upon ingestion. Our findings indicated that E 171 showed higher absolute values of ζ potential in artificial intestinal juice than in water, artificial saliva, or artificial gastric juice, implying enhanced stability in artificial intestinal juice [70]. It was observed that during the intestinal digestion stage, E 171 released nanoparticles. These results are consistent with our previous study on food-grade nanosilica, which also released more nanoparticles during the intestinal fluid digestion phase [28]. This implies that the intestinal digestion phase is the main stage of nanoparticle release from food-grade nanomaterials. The liberation of nanoparticles from E 171 within the intestinal tract is likely a contributing factor to its induction of intestinal toxicity. Previous studies have identified various adverse effects of E 171 on the intestinal tract, including impairment of intestinal immune homeostasis [16], worsening of pre-existing intestinal disease [71], an increase in colonic adenomas [17], and alteration of the composition of the intestinal bacteria [72].

Beyond intestinal toxicity, it is particularly significant that E 171 may be absorbed from the intestines into the bloodstream, potentially affecting multiple organs, including the liver. Our study revealed the accumulation of E 171 in the small intestine and liver. In line with our findings, a previous study showed that food-grade TiO_2 particles were present in the liver, small intestine, and colons of Wistar rats after 7 days of E 171 gavage (10 mg/kg bw per day), with the highest density of Ti found near the portal vein [16]. A significant elevation of Ti levels in the liver and colon was detected after repeated oral administration of E 171 suspension to mice (5 mg/kg bw for 3 days/week for 3 weeks) [30]. Similarly, the Ti concentration in the liver increased after a single intravenous injection of E 171 (6 mg/kg bw per day) [31]. However, in these studies, E 171 was given by gavage or injection, and the in vivo distribution of E 171 when mixed with food was not investigated. Our results suggested that E 171 can enter the liver through blood circulation even when mixed with food containing complex components such as sugars and protein. In addition, our study elucidated the impact of E 171 on the liver over varying exposure durations at human-relevant doses. Specifically, a 28-day exposure period to E 171 elicited no notable pathological alterations in the liver. In contrast, an 84-day exposure period was associated with the onset of liver injury and inflammatory reactions.

More importantly, oral exposures of 28 and/or 84 days to E 171 induced alterations in methylation and hydroxymethylation levels in mouse liver DNA. Previous studies have demonstrated that E 171 induced global DNA methylation alterations in mouse colonic epithelial cells [15] and TiO_2 nanoparticles have been observed to cause a reduction in global DNA methylation levels across various cells in vitro, including colon, liver, lung, and skin cells [73–75]. Combined with our findings, it appears that E 171 could exert a broad spectrum of effects on DNA methylation. It was worth noting that previous studies have focused on assessing the global DNA methylation changes induced by E 171 or TiO_2 nanoparticles. Our study, however, has provided further evidence that 84 days of E 171 oral exposure results in DNA methylation alterations in both CG and non-CG contexts in the mouse liver, with the non-CG context showing more substantial changes, as determined by WGBS. Our research delineated a marked augmentation in DNA methylation levels in the region near the ~ 8 kb position within the non-CG gene body, instigated by E 171 exposure. To our knowledge, this phenomenon has not been previously explored; hence, we advocate for a comprehensive investigation into the methylation alterations induced by E 171. Recent studies have provided evidence of the wide distribution and importance of non-CG environments in mammals, including gene expression regulation and chromosomal interactions [76–78]. Importantly, our previous studies and other reports have demonstrated that nanomaterials such as food-grade nanosilica or graphene oxide can alter methylation levels in non-CG contexts, as evidenced by the liver of mice exposed to these substances [28, 29, 79]. Our findings indicated that E 171 may also affect CG and non-CG methylation levels. Therefore, we need further studies to examine the effects of nanomaterials on both CG and non-CG methylation.

Drawing on research into E 171-induced DNA methylation changes within CG and non-CG contexts, our study uncovered that E 171 initiates ferroptosis through the regulation of NCOA4-mediated ferritinophagy. NCOA4 is a cargo receptor for ferritin degradation and plays a

key role in ferritinophagy [80]. Upregulation of NCOA4 expression facilitates ferritinophagy and subsequent ferroptosis [81]. During ferritinophagy, NCOA4 directly binds to FTH1 and transports the ferritin complex to the lysosome, where the degraded ferritin releases free iron [82]. Autophagy positively regulates ferroptosis by modulating iron homeostasis through NCOA4-mediated ferritinophagy [33]. Our results showed that autophagy was activated in mouse liver after 84 days of E 171 exposure, as indicated by the increased expression of LC3B protein. Interestingly, the expression of the autophagy substrate p62 also increased, contrary to the usual decrease during autophagy activation. Previous studies reported that the elevation of p62 also occurred in mouse liver with hepcidin knockout-induced ferroptosis and in lung epithelial cells with polystyrene nanoparticles-induced ferroptosis [49, 83]. This phenomenon might result from the unique role of p62 in ferritinophagy, as p62 can act as a platform to tether NCOA4 to LC3 and promote ferritinophagy, and p62 overexpression can promote ferritinophagy [84]. Therefore, our findings indicated that the methylation reduction induced by E 171 increased the expression of NCOA4, p62, and LC3B in mouse liver after 84 days of exposure. Under the effect of p62, NCOA4 bound to LC3B and transported ferritin to the lysosome by binding to FTH1, degrading ferritin, and inducing ferroptosis. Our investigation demonstrated that E 171 induces ferroptosis in liver tissues and elicits detrimental hepatic effects, underscoring the necessity for a further evaluation of substances that activate ferroptosis.

Nanoparticles have been widely used to induce ferroptosis in tumor cells for the treatment of cancer, but the toxic effects of nanoparticle-induced ferroptosis in normal cells should not be overlooked [85, 86]. Iron homeostasis disruption may be a critical mechanism for nanomaterial-induced ferroptosis. For instance, alumina nanoparticles, graphene quantum dots, and silica nanoparticles disrupted iron balance and induced ferroptosis in neurons and microglia, respectively [52, 87, 88]. Polystyrene nanoplastics, zinc oxide nanoparticles, and MoS_2 nanosheets triggered iron imbalance and ferroptosis through NCOA4-mediated ferritinophagy [49, 89, 90]. These studies, along with our results, indicated that NCOA4-mediated ferritinophagy and the subsequent iron homeostasis disruption are crucial steps in nanomaterial-induced ferroptosis. Our study unveiled a novel potential mechanism for nanomaterial-induced ferroptosis, namely, nanomaterials modulate the expression of key proteins in ferritinophagy by altering DNA methylation levels, thus enhancing ferroptosis. Epigenetic modifications can determine the vulnerability of cancer cells to ferroptosis through transcriptional and translational mechanisms [42]. Concurrently, the activation of ferroptosis by nanomaterials constitutes a significant strategy for cancer therapy [91]. Therefore, a thorough understanding of the influence of epigenetic modifications, especially DNA methylation, on nanomaterial-induced ferroptosis could advance the application of nanomaterials in cancer treatment.

It is worth noting that although E 171 was homogeneously dispersed as a powder in mouse feed, the process of preparing mouse feed differed from that of human food. This difference may have impacted the relatively milder toxic effects observed for E 171 in this study [13]. Therefore, future studies should consider adding E 171 in a manner that more closely resembles human food preparation, such as dispersing E 171 initially in a liquid medium followed by mixing it with feed using an appropriate dispersion program [92]. In addition, because the toxicokinetics of nanomaterials differ from those of conventional chemicals, the specificity of nanomaterials including no partitioning equilibrium but macrophage-mediated distribution should be considered when performing animal and human dose conversions [93, 94].

Conclusions

The present study revealed potential hepatotoxic effects of E 171 in vivo and demonstrated that both subacute and subchronic exposure to E 171 resulted in global changes in DNA methylation and hydroxymethylation in the liver of mice. Moreover, subchronic exposure to E 171 induced hepatic inflammation and altered plasma lipid levels. WGBS results revealed aberrant DNA methylation patterns in the context of mCG, mCHG, and mCHH triggered by E 171 in mouse liver. Notably, ferroptosis was significantly enriched in pathway enrichment analyses based on DMGs, and subsequent experiments verified the activation of ferroptosis in the liver upon subchronic exposure to E 171. Mechanistically, E 171 altered DNA methylation levels and increased the expression of NCOA4, p62, and LC3B, which promoted ferritinophagy and caused iron imbalance, leading to further ferroptosis. Overall, this study assessed the epigenetic effects of E 171 on mouse liver under a simulated human exposure condition and showed that E 171-induced epigenetic alterations triggered ferroptosis in the liver through NCOA4-mediated ferritinophagy, providing an epigenetic reference for the safety assessment of E 171. Given that E 171 may reach other organs through the bloodstream, its broader effects on other vital organs, especially epigenetic effects, warrant further evaluation.

Abbreviations

TiO_2	Titanium dioxide
E 171	Food- and pharmaceutical-grade TiO_2
EU	European Union

EFSA	European Food Safety Authority
NCOA4	Nuclear receptor coactivator 4
GPX4	Glutathione peroxidase 4
Nrf2	Nuclear factor E2-related factor 2
WGBS	Whole genome bisulfite sequencing
Fmin	Minimum Feret diameter
Fmax	Maximum Feret diameter
Fmean	Mean Feret diameter
PSDs	Particle size distributions
ddH_2O	Double-distilled water
d_H	Hydrodynamic diameter
DLS	Dynamic light scattering
ELS	Electrophoretic light scattering
H&E	Hematoxylin and Eosin
STEM	Scanning transmission electron microscopy
5-mC	5-Methylcytosine
5-hmC	5-Hydroxymethylcytosine
RT-qPCR	Quantitative reverse transcription polymerase chain reaction
SD	Standard deviation
SEM	Scanning electron microscopy
TEM	Transmission electron microscopy
XRD	X-ray powder diffractometry
PDI	Polydispersity index
ALT	Alanine transaminase
AST	Aspartate transaminase
TG	Triglycerides
TC	Total cholesterol
TBIL	Total bilirubin
EDS	Energy dispersive X-ray spectroscopy
TSS	Transcription start sites
TES	Transcription termination sites
DMS	Differentially methylated site
DSS	Dispersion Shrinkage for Sequencing data
DMR	Differentially methylated region
GO	Gene Ontology
KEGG	Kyoto Encyclopedia of Genes and Genomes

Supplementary Information

The online version contains supplementary material available at https://doi.org/10.1186/s12989-024-00598-2.

Additional file 1.

Additional file 2.

Acknowledgements
We thank D. S. and G. Z. in the Center of Cryo-Electron Microscopy (CCEM), Zhejiang University for their technical assistance on Scanning Electron Microscopy.

Author contributions
JS and JY contributed equally to this work. JS, JY, and HL performed experiments. JS, XL, and JY drafted the manuscript. JS, JY, RS, and YZ contributed to the data analysis and interpretation. XL and XF designed the study. All the authors have critically revised the manuscript. All authors have read, reviewed, and approved the final manuscript as submitted to take public responsibility for it.

Funding
This work was supported by the Zhejiang Provincial Natural Science Foundation of China (No. LY23B070004), and the National Natural Science Foundation of China (No. 82374136).

Data availability
The datasets supporting the conclusions of this article are included within the article and can be retrieved from the corresponding author upon reasonable request.

Declarations

Ethics approval and consent to participate
All procedures and experiments on animals were performed under the guidelines of the Animal Care and Use Committee of Zhejiang University School of Medicine and followed the guidelines covered in the Use of Animals in Toxicology.

Consent for publication
Not applicable.

Competing interests
The authors declare no competing financial interest.

Author details
[1]Pharmaceutical Informatics Institute, College of Pharmaceutical Sciences, Zhejiang University, Hangzhou 310058, China. [2]State Key Laboratory of Chinese Medicine Modernization, Innovation Center of Yangtze River Delta, Zhejiang University, Jiaxing 314102, China. [3]Jinhua Institute of Zhejiang University, Jinhua 321299, China. [4]The Joint-Laboratory of Clinical Multi-Omics Research between Zhejiang University and Ningbo Municipal Hospital of TCM, Ningbo Municipal Hospital of TCM, Ningbo 315010, China. [5]Department of Infectious Diseases, The Second Affiliated Hospital, Zhejiang University School of Medicine, Hangzhou 310009, China.

Received: 20 March 2024 Accepted: 6 September 2024
Published online: 18 September 2024

References

1. Winkler HC, Notter T, Meyer U, Naegeli H. Critical review of the safety assessment of titanium dioxide additives in food. J Nanobiotechnol. 2018;16(1):51.
2. Aguilar F, Crebelli R, Di Domenico A, Dusemund B, Frutos MJ, Galtier P, et al. Re-evaluation of titanium dioxide (E 171) as a food additive. EFSA J. 2016;14(9):4545.
3. European Medicines Agency. Final feedback from european medicine agency (EMA) to the EU commission request to evaluate the impact of the removal of titanium dioxide from the list of authorised food additives on medicinal products. European Medicines Agency. 2021. https://www.Ema.Europa.Eu/En/Documents/Report/Final-Feedback-European-Medicine-Agency-Ema-Eu-Commission-Request-Evaluate-Impact-Removal-Titanium_En.Pdf. Accessed 12 April 2023.
4. Cao X, Han Y, Gu M, Du H, Song M, Zhu X, et al. Foodborne titanium dioxide nanoparticles induce stronger adverse effects in obese mice than non-obese mice: gut microbiota dysbiosis, colonic inflammation, and proteome alterations. Small. 2020;16(36): e2001858.
5. Weir A, Westerhoff P, Fabricius L, Hristovski K, von Goetz N. Titanium dioxide nanoparticles in food and personal care products. Environ Sci Technol. 2012;46(4):2242–50.
6. Younes M, Aquilina G, Castle L, Engel KH, Fowler P, Frutos FM, et al. Scientific opinion on the proposed amendment of the EU specifications for titanium dioxide (E 171) with respect to the inclusion of additional parameters related to its particle size distribution. EFSA J. 2019;17(7): e05760.
7. European Commission. Directorate-General for Health and Food Safety. Commission regulation (EU) 2022/63 of 14 January 2022 amending annexes II and III to regulation (EC) No 1333/2008 of the european parliament and of the council as regards the food additive titanium dioxide (E 171) (text with EEA relevance). European Commission. 2022. http://Data.Europa.Eu/Eli/Reg/2022/63/Oj. Accessed 12 April 2023.
8. Younes M, Aquilina G, Castle L, Engel KH, Fowler P, Frutos FM, et al. Safety assessment of titanium dioxide (E171) as a food additive. EFSA J. 2021;19(5): e06585.
9. United States Department of Agriculture, Global Agriculture Information Network. Titanium dioxide banned as a food additive in the EU. United States Department of Agriculture. 2022. https://Fas.Usda.Gov/Data/European-Union-Titanium-Dioxide-Banned-Food-Additive-Eu. Accessed 12 April 2023.

10. Committee on Toxicity, Food Standards Agency. Interim position paper on titanium dioxide. Committee on Toxicity. 2022. https://Cot.Food.Gov.Uk/Sites/Default/Files/2022-01/Tio2%20Cot%20Interim%20Position%20Paper.Pdf. Accessed 12 April 2023.
11. Health Canada. State of the science of titanium dioxide (TiO_2) as a food additive. Health Canada. 2022. https://www.Canada.Ca/En/Health-Canada/Services/Food-Nutrition/Reports-Publications/Titanium-Dioxide-Food-Additive-Science-Report.Html. Accessed 12 April 2023.
12. World Health Organization, Joint FAO/WHO Expert Committee on Food Additives. JECFA's risk assessment of titanium dioxide risk released – background information. World Health Organization. 2023. https://cdn.who.int/media/docs/default-source/food-safety/jecfa/summary-and-conclusions/jecfa-riskassemsent-of-titanium-dioxide-released.pdf. Accessed 4 March 2024.
13. Ferraris F, Raggi A, Ponti J, Mehn D, Gilliland D, Savini S, et al. Agglomeration behavior and fate of food-grade titanium dioxide in human gastrointestinal digestion and in the lysosomal environment. Nanomaterials. 2023;13(13):1908.
14. Pele LC, Thoree V, Bruggraber SF, Koller D, Thompson RP, Lomer MC, et al. Pharmaceutical/food grade titanium dioxide particles are absorbed into the bloodstream of human volunteers. Part Fibre Toxicol. 2015;12:26.
15. Carle C, Boucher D, Morelli L, Larue C, Ovtchinnikova E, Battut L, et al. Perinatal foodborne titanium dioxide exposure-mediated dysbiosis predisposes mice to develop colitis through life. Part Fibre Toxicol. 2023;20(1):45.
16. Bettini S, Boutet-Robinet E, Cartier C, Coméra C, Gaultier E, Dupuy J, et al. Food-grade TiO_2 impairs intestinal and systemic immune homeostasis, initiates preneoplastic lesions and promotes aberrant crypt development in the rat colon. Sci Rep. 2017;7(1):40373.
17. Medina-Reyes EI, Delgado-Buenrostro NL, Diaz-Urbina D, Rodriguez-Ibarra C, Deciga-Alcaraz A, Gonzalez MI, et al. Food-grade titanium dioxide (E171) induces anxiety, adenomas in colon and goblet cells hyperplasia in a regular diet model and microvesicular steatosis in a high fat diet model. Food Chem Toxicol. 2020;146: 111786.
18. Jensen DM, Lohr M, Sheykhzade M, Lykkesfeldt J, Wils RS, Loft S, et al. Telomere length and genotoxicity in the lung of rats following intragastric exposure to food-grade titanium dioxide and vegetable carbon particles. Mutagenesis. 2019;34(2):203–14.
19. Li J, Chen C, Xia T. Understanding nanomaterial-liver interactions to facilitate the development of safer nanoapplications. Adv Mater. 2022;34(11): e2106456.
20. Liu H, Lai W, Liu X, Yang H, Fang Y, Tian L, et al. Exposure to copper oxide nanoparticles triggers oxidative stress and endoplasmic reticulum (ER)-stress induced toxicology and apoptosis in male rat liver and BRL-3A cell. J Hazard Mater. 2021;401: 123349.
21. Zhang B, Fan X, Du H, Zhao M, Zhang Z, Zhu R, et al. Foodborne carbon dot exposure induces insulin resistance through gut microbiota dysbiosis and damaged intestinal mucus layer. ACS Nano. 2023;17(6):6081–94.
22. Feil R, Fraga MF. Epigenetics and the environment: emerging patterns and implications. Nat Rev Genet. 2012;13(2):97–109.
23. Bicho RC, Roelofs D, Marien J, Scott-Fordsmand JJ, Amorim M. Epigenetic effects of (nano)materials in environmental species - Cu case study in enchytraeus crypticus. Environ Int. 2020;136: 105447.
24. Chen Y, Xu M, Zhang J, Ma J, Gao M, Zhang Z, et al. Genome-wide DNA methylation variations upon exposure to engineered nanomaterials and their implications in nanosafety assessment. Adv Mater. 2017;29(6):1604580.
25. Chen C, Li YF, Qu Y, Chai Z, Zhao Y. Advanced nuclear analytical and related techniques for the growing challenges in nanotoxicology. Chem Soc Rev. 2013;42(21):8266–303.
26. Hu J, Lin W, Lin B, Wu K, Fan H, Yu Y. Persistent DNA methylation changes in zebrafish following graphene quantum dots exposure in surface chemistry-dependent manner. Ecotoxicol Environ Saf. 2019;169:370–5.
27. Wu Y, Feng W, Liu R, Xia T, Liu S. Graphene oxide causes disordered zonation due to differential intralobular localization in the liver. ACS Nano. 2020;14(1):877–90.
28. Lu X, Li J, Lou H, Cao Z, Fan X. Genome-wide DNA methylation alterations and potential risk induced by subacute and subchronic exposure to food-grade nanosilica in mice. ACS Nano. 2021;15(5):8225–43.
29. Zhan Y, Lou H, Shou R, Li A, Shang J, Jin Y, et al. Maternal exposure to E 551 during pregnancy leads to genome-wide DNA methylation changes and metabolic disorders in the livers of pregnant mice and their fetuses. J Hazard Mater. 2024;465: 133233.
30. Talamini L, Gimondi S, Violatto MB, Fiordaliso F, Pedica F, Tran NL, et al. Repeated administration of the food additive E171 to mice results in accumulation in intestine and liver and promotes an inflammatory status. Nanotoxicology. 2019;13(8):1087–101.
31. Sitia G, Fiordaliso F, Violatto MB, Alarcon JF, Talamini L, Corbelli A, et al. Food-grade titanium dioxide induces toxicity in the nematode caenorhabditis elegans and acute hepatic and pulmonary responses in mice. Nanomaterials. 2022;12(10):1669.
32. Heringa MB, Peters RJB, Bleys RLAW, van der Lee MK, Tromp PC, van Kesteren PCE, et al. Detection of titanium particles in human liver and spleen and possible health implications. Part Fibre Toxicol. 2018;15(1):15.
33. Gao M, Monian P, Pan Q, Zhang W, Xiang J, Jiang X. Ferroptosis is an autophagic cell death process. Cell Res. 2016;26(9):1021–32.
34. Dixon SJ, Lemberg KM, Lamprecht MR, Skouta R, Zaitsev EM, Gleason CE, et al. Ferroptosis: an iron-dependent form of nonapoptotic cell death. Cell. 2012;149(5):1060–72.
35. Jiang X, Stockwell BR, Conrad M. Ferroptosis: mechanisms, biology and role in disease. Nat Rev Mol Cell Bio. 2021;22(4):266–82.
36. Stockwell BR. Ferroptosis turns 10: emerging mechanisms, physiological functions, and therapeutic applications. Cell. 2022;185(14):2401–21.
37. Mancardi D, Mezzanotte M, Arrigo E, Barinotti A, Roetto A. Iron overload, oxidative stress, and ferroptosis in the failing heart and liver. Antioxidants. 2021;10(12):1864.
38. Tsurusaki S, Tsuchiya Y, Koumura T, Nakasone M, Sakamoto T, Matsuoka M, et al. Hepatic ferroptosis plays an important role as the trigger for initiating inflammation in nonalcoholic steatohepatitis. Cell Death Dis. 2019;10(6):449.
39. Kim JW, Lee JY, Oh M, Lee EW. An integrated view of lipid metabolism in ferroptosis revisited via lipidomic analysis. Exp Mol Med. 2023;55(8):1620–31.
40. Gautheron J, Gores GJ, Rodrigues C. Lytic cell death in metabolic liver disease. J Hepatol. 2020;73(2):394–408.
41. Crichton RR. Ferritin: structure, synthesis and function. N Engl J Med. 1971;284(25):1413–22.
42. Wang Y, Hu J, Wu S, Fleishman JS, Li Y, Xu Y, et al. Targeting epigenetic and posttranslational modifications regulating ferroptosis for the treatment of diseases. Signal Transduct Target Ther. 2023;8(1):449.
43. Wang X, Kong X, Feng X, Jiang DS. Effects of DNA, RNA, and protein methylation on the regulation of ferroptosis. Int J Biol Sci. 2023;19(11):3558–75.
44. Fullgrabe J, Klionsky DJ, Joseph B. The return of the nucleus: transcriptional and epigenetic control of autophagy. Nat Rev Mol Cell Bio. 2014;15(1):65–74.
45. Zhang Z, Fu C, Liu J, Sai X, Qin C, Di T, et al. Hypermethylation of the Nrf2 promoter induces ferroptosis by inhibiting the Nrf2-GPX4 axis in COPD. Int J Chronic Obstruct Pulm Dis. 2021;16:3347–62.
46. Lan T, Sun TT, Wei C, Cheng T, Yang F, Zhang JN, et al. Epigenetic regulation of ferroptosis in central nervous system diseases. Mol Neurobiol. 2023;60(7):3584–99.
47. Suzuki T, Komatsu T, Shibata H, Tanioka A, Vargas D, Kawabata-Iwakawa R, et al. Crucial role of iron in epigenetic rewriting during adipocyte differentiation mediated by JMJD1A and TET2 activity. Nucleic Acids Res. 2023;51(12):6120–42.
48. Gu C, Chang W, Wu J, Yao Y, Liu G, Yuan Y, et al. NCOA4: an immunomodulation-related prognostic biomarker in colon adenocarcinoma and pan-cancer. J Oncol. 2022;2022:5242437.
49. Yang S, Zhang T, Ge Y, Cheng Y, Yin L, Pu Y, et al. Ferritinophagy mediated by oxidative stress-driven mitochondrial damage is involved in the polystyrene nanoparticles-induced ferroptosis of lung injury. ACS Nano. 2023;17(24):24988–5004.
50. Tang J, Bu W, Hu W, Zhao Z, Liu L, Luo C, et al. Ferroptosis is involved in sex-specific small intestinal toxicity in the offspring of adult mice exposed to polystyrene nanoplastics during pregnancy. ACS Nano. 2023;17(3):2440–9.
51. Ma Y, Ding X, Liu Q, Pang Y, Cao Y, Zhang T. Safety assessment of graphene oxide and microcystin-LR complex: a toxicological scenario beyond physical mixture. Part Fibre Toxicol. 2022;19(1):26.
52. Zhang H, Jiao W, Cui H, Sun Q, Fan H. Combined exposure of alumina nanoparticles and chronic stress exacerbates hippocampal neuronal

ferroptosis via activating IFN-γ/ASK1/JNK signaling pathway in rats. J Hazard Mater. 2021;411: 125179.
53. More S, Bampidis V, Benford D, Bragard C, Halldorsson T, Hernandez-Jerez A, et al. Guidance on technical requirements for regulated food and feed product applications to establish the presence of small particles including nanoparticles. EFSA J. 2021;19(8): e06769.
54. Bresch H, Hodoroaba VD, Schmidt A, Rasmussen K, Rauscher H. Counting small particles in electron microscopy images-proposal for rules and their application in practice. Nanomaterials. 2022;12(13):2238.
55. Nair AB, Jacob S. A simple practice guide for dose conversion between animals and human. J Basic Clin Pharm. 2016;7(2):27–31.
56. Zhu M, Nie G, Meng H, Xia T, Nel A, Zhao Y. Physicochemical properties determine nanomaterial cellular uptake, transport, and fate. Acc Chem Res. 2013;46(3):622–31.
57. Musial J, Krakowiak R, Mlynarczyk DT, Goslinski T, Stanisz BJ. Titanium dioxide nanoparticles in food and personal care products - what do we know about their safety? Nanomaterials. 2020;10(6):1110.
58. Li C, Zhang R, Ma C, Shang H, McClements DJ, White JC, et al. Food-grade titanium dioxide particles decreased the bioaccessibility of vitamin D3 in the simulated human gastrointestinal tract. J Agric Food Chem. 2021;69(9):2855–63.
59. Zhu X, Zhao L, Wang Y, Hu X, Zhu Y, Yang X. Dietary titanium dioxide particles (E171) promote diet-induced atherosclerosis through reprogramming gut microbiota-mediated choline metabolism in $APOE^{-/-}$ mice. J Hazard Mater. 2022;436: 129179.
60. Faust JJ, Doudrick K, Yang Y, Westerhoff P, Capco DG. Food grade titanium dioxide disrupts intestinal brush border microvilli in vitro independent of sedimentation. Cell Biol Toxicol. 2014;30(3):169–88.
61. Lu HY, Wang YJ, Hou WC. Bioaccumulation and depuration of TiO_2 nanoparticles by zebrafish through dietary exposure: size- and number concentration-resolved analysis using single-particle ICP-MS. J Hazard Mater. 2022;426: 127801.
62. Lu X, Miousse IR, Pirela SV, Melnyk S, Koturbash I, Demokritou P. Short-term exposure to engineered nanomaterials affects cellular epigenome. Nanotoxicology. 2016;10(2):140–50.
63. Greenberg M, Bourc'His D. The diverse roles of DNA methylation in mammalian development and disease. Nat Rev Mol Cell Biol. 2019;20(10):590–607.
64. Kotronen A, Vehkavaara S, Seppala-Lindroos A, Bergholm R, Yki-Jarvinen H. Effect of liver fat on insulin clearance. Am J Physiol-Endoc M. 2007;293(6):E1709–15.
65. Lu M, Wan M, Leavens KF, Chu Q, Monks BR, Fernandez S, et al. Insulin regulates liver metabolism in vivo in the absence of hepatic Akt and Foxo1. Nat Med. 2012;18(3):388–95.
66. Liu Z, Cordoba-Chacon J, Kineman RD, Cronstein BN, Muzumdar R, Gong Z, et al. Growth hormone control of hepatic lipid metabolism. Diabetes. 2016;65(12):3598–609.
67. Hanaire-Broutin H, Sallerin-Caute B, Poncet MF, Tauber M, Bastide R, Rosenfeld R, et al. Insulin therapy and GH-IGF-I axis disorders in diabetes: impact of glycaemic control and hepatic insulinization. Diabetes Metab. 1996;22(4):245–50.
68. Kolaczynski JW, Caro JF. Insulin-like growth factor-1 therapy in diabetes: physiologic basis, clinical benefits, and risks. Ann Intern Med. 1994;120(1):47–55.
69. Li J, Zheng Y, Yan P, Song M, Wang S, Sun L, et al. A single-cell transcriptomic atlas of primate pancreatic islet aging. Natl Sci Rev. 2020;8(2):nwaa127.
70. Bhattacharjee S. DLS and zeta potential - What they are and what they are not? J Control Release. 2016;235:337–51.
71. Urrutia-Ortega IM, Garduño-Balderas LG, Delgado-Buenrostro NL, Freyre-Fonseca V, Flores-Flores JO, González-Robles A, et al. Food-grade titanium dioxide exposure exacerbates tumor formation in colitis associated cancer model. Food Chem Toxicol. 2016;93:20–31.
72. Baranowska-Wójcik E, Szwajgier D, Gustaw K. Effect of TiO_2 on selected pathogenic and opportunistic intestinal bacteria. Biol Trace Elem Res. 2022;200(5):2468–74.
73. Pogribna M, Koonce NA, Mathew A, Word B, Patri AK, Lyn-Cook B, et al. Effect of titanium dioxide nanoparticles on DNA methylation in multiple human cell lines. Nanotoxicology. 2020;14(4):534–53.
74. Sierra MI, Rubio L, Bayon GF, Cobo I, Menendez P, Morales P, et al. DNA methylation changes in human lung epithelia cells exposed to multi-walled carbon nanotubes. Nanotoxicology. 2017;11(7):857–70.
75. Ghosh M, Oner D, Duca RC, Cokic SM, Seys S, Kerkhofs S, et al. Cyto-genotoxic and DNA methylation changes induced by different crystal phases of TiO_2-np in bronchial epithelial (16-HBE) cells. Mutat Res. 2017;796:1–12.
76. Xie W, Barr CL, Kim A, Yue F, Lee AY, Eubanks J, et al. Base-resolution analyses of sequence and parent-of-origin dependent DNA methylation in the mouse genome. Cell. 2012;148(4):816–31.
77. Guo JU, Su Y, Shin JH, Shin J, Li H, Xie B, et al. Distribution, recognition and regulation of non-CpG methylation in the adult mammalian brain. Nat Neurosci. 2014;17(2):215–22.
78. Rizzardi LF, Hickey PF, Rodriguez DV, Tryggvadottir R, Callahan CM, Idrizi A, et al. Neuronal brain-region-specific DNA methylation and chromatin accessibility are associated with neuropsychiatric trait heritability. Nat Neurosci. 2019;22(2):307–16.
79. Ku T, Hao F, Yang X, Rao Z, Liu QS, Sang N, et al. Graphene quantum dots disrupt embryonic stem cell differentiation by interfering with the methylation level of *Sox2*. Environ Sci Technol. 2021;55(5):3144–55.
80. Mancias JD, Wang X, Gygi SP, Harper JW, Kimmelman AC. Quantitative proteomics identifies NCOA4 as the cargo receptor mediating ferritinophagy. Nature. 2014;509(7498):105–9.
81. Hou W, Xie Y, Song X, Sun X, Lotze MT, Zeh HR, et al. Autophagy promotes ferroptosis by degradation of ferritin. Autophagy. 2016;12(8):1425–8.
82. Dowdle WE, Nyfeler B, Nagel J, Elling RA, Liu S, Triantafellow E, et al. Selective VPS34 inhibitor blocks autophagy and uncovers a role for NCOA4 in ferritin degradation and iron homeostasis in vivo. Nat Cell Biol. 2014;16(11):1069–79.
83. Lunova M, Goehring C, Kuscuoglu D, Mueller K, Chen Y, Walther P, et al. Hepcidin knockout mice fed with iron-rich diet develop chronic liver injury and liver fibrosis due to lysosomal iron overload. J Hepatol. 2014;61(3):633–41.
84. Liu L, Zheng B, Luo M, Du J, Yang F, Huang C, et al. Suppression of USP8 sensitizes cells to ferroptosis via SQSTM1/p62-mediated ferritinophagy. Protein Cell. 2023;14(3):230–4.
85. Kim SE, Zhang L, Ma K, Riegman M, Chen F, Ingold I, et al. Ultrasmall nanoparticles induce ferroptosis in nutrient-deprived cancer cells and suppress tumour growth. Nat Nanotechnol. 2016;11(11):977–85.
86. Zhu L, You Y, Zhu M, Song Y, Zhang J, Hu J, et al. Ferritin-hijacking nanoparticles spatiotemporally directing endogenous ferroptosis for synergistic anticancer therapy. Adv Mater. 2022;34(51): e2207174.
87. Wu T, Liang X, Liu X, Li Y, Wang Y, Kong L, et al. Induction of ferroptosis in response to graphene quantum dots through mitochondrial oxidative stress in microglia. Part Fibre Toxicol. 2020;17(1):30.
88. Hou S, Li C, Wang Y, Sun J, Guo Y, Ning X, et al. Silica nanoparticles cause activation of NLRP3 inflammasome in-vitro model-using microglia. Int J Nanomed. 2022;17:5247–64.
89. Qin X, Zhang J, Wang B, Xu G, Yang X, Zou Z, et al. Ferritinophagy is involved in the zinc oxide nanoparticles-induced ferroptosis of vascular endothelial cells. Autophagy. 2021;17(12):4266–85.
90. Liu B, Jiang W, Ye Y, Liu L, Wei X, Zhang Q, et al. 2D MoS_2 nanosheets induce ferroptosis by promoting NCOA4-dependent ferritinophagy and inhibiting ferroportin. Small. 2023;19(24): e2208063.
91. Yang H, Yao X, Liu Y, Shen X, Li M, Luo Z. Ferroptosis nanomedicine: clinical challenges and opportunities for modulating tumor metabolic and immunological landscape. ACS Nano. 2023;17(16):15328–53.
92. More S, Bampidis V, Benford D, Bragard C, Halldorsson T, Hernandez-Jerez A, et al. Guidance on risk assessment of nanomaterials to be applied in the food and feed chain: human and animal health. EFSA J. 2021;19(8): e06768.
93. Chen Q, Riviere JE, Lin Z. Toxicokinetics, dose-response, and risk assessment of nanomaterials: methodology, challenges, and future perspectives. Wiley Interdiscip Rev Nanomed Nanobiotechnol. 2022;14(6): e1808.
94. Zuckerman JE, Gritli I, Tolcher A, Heidel JD, Lim D, Morgan R, et al. Correlating animal and human phase Ia/Ib clinical data with CALAA-01, a targeted, polymer-based nanoparticle containing siRNA. Proc Natl Acad Sci U S A. 2014;111(31):11449–54.

Publisher's Note